Accepted Manuscript

Oxidative polymerization of 5-hydroxytryptamine to physically and chemically immobilize glucose oxidase for electrochemical biosensing

Ting Huang, Zaichun Liu, Yunlong Li, Yanqiu Li, Long Chao, Chao Chen, Yueming Tan, Qingji Xie, Shouzhuo Yao, Yuping Wu

PII: S0003-2670(18)30209-5

DOI: 10.1016/j.aca.2018.02.020

Reference: ACA 235736

To appear in: *Analytica Chimica Acta*

Received Date: 12 August 2017

Accepted Date: 9 February 2018

Please cite this article as: T. Huang, Z. Liu, Y. Li, Y. Li, L. Chao, C. Chen, Y. Tan, Q. Xie, S. Yao, Y. Wu, Oxidative polymerization of 5-hydroxytryptamine to physically and chemically immobilize glucose oxidase for electrochemical biosensing, *Analytica Chimica Acta* (2018), doi: 10.1016/j.aca.2018.02.020.

Graphical Abstract

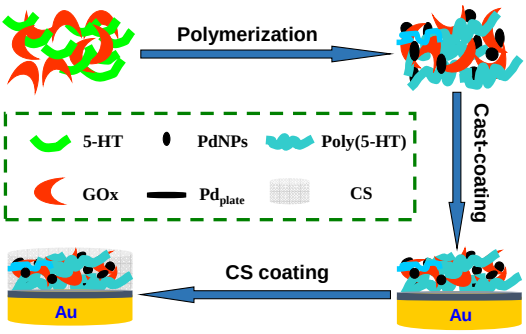

Oxidative polymerization of 5-hydroxytryptamine to physically and chemically immobilize glucose oxidase for electrochemical biosensing

Ting Huang[a], Zaichun Liu[b], Yunlong Li[a], Yanqiu Li[a], Long Chao[a], Chao Chen[a], Yueming Tan[a], Qingji Xie[a,*], Shouzhuo Yao[a], Yuping Wu[b,*]

[a] Key Laboratory of Chemical Biology & Traditional Chinese Medicine Research (Ministry of Education of China), College of Chemistry and Chemical Engineering, Hunan Normal University, Changsha 410081, China

[b] School of Energy Science and Engineering & Institute of Advanced Materials, Nanjing Tech University, Nanjing 211816, Jiangsu Province (China)

[*]Corresponding authors. Tel: +86-731-88865515.
E-mail address: xieqj@hunnu.edu.cn (Q.J. Xie), wuyp@fudan.edu.cn (Y.P. Wu)

ABSTRACT

Poly(5-hydroxytryptamine) (poly(5-HT)) is exploited as a new and efficient enzyme-immobilization matrix for amperometric and biofuel cell (BFC)-based biosensing. A GOx-poly(5-HT)-Pd nanoparticles (PdNPs) bionanocomposite is prepared by Na_2PdCl_4-initiated oxidized polymerization of 5-hydroxytryptamine (5-HT) in a neutral aqueous solution containing glucose oxidase (GOx), and this bionanocomposite and then chitosan (CS) are cast-coated on a Pd-plated Au electrode to yield a CS/GOx-poly(5-HT)-PdNPs/Pd_{plate}/Au enzyme electrode. Scanning/transmission electron microscopy, UV-vis spectrophotometry and electrochemical quartz crystal microbalance are employed for material characterization and/or process monitoring. Under optimized conditions, the amperometric response of the enzyme electrode is linear with glucose concentration from 2.0 μM to 6.66 mM with a sensitivity of 110 μA mM^{-1} cm^{-2}, a limit of detection of 0.2 μM, and excellent operation/storage stability in the first-generation biosensing mode. The sensitivity is larger than those of some conventional electrodes under identical conditions. The enzyme electrode also works well in the second-generation biosensing mode. By using the enzyme electrode as the anode for glucose oxidation and a Pd_{plate}/Au electrode as the cathode for $KMnO_4$ reduction, a monopolar BFC is constructed as a self-powered biosensor, the current response of which is linear with glucose concentration from 50 μM to 34.5 mM. Experiments also show that poly(5-HT) is a physical and chemical dual-immobilization matrix of enzyme, since the abundant amino groups in poly(5-HT) can be used for chemical bonding of GOx.

Keywords: Poly(5-hydroxytryptamine); Glucose oxidase; Pd nanoparticles; Glucose biosensing; Biofuel cell

1. Introduction

5-Hydroxytryptamine (serotonin, 5-HT) as a monoamine neurotransmitter contains one amino group that is connected to an aromatic ring by a two-carbon chain (-CH_2-CH_2-). 5-HT is widely dispersed throughout the central nervous system and plays a vital role in the regulation of appetite, sleep, memory, learning and body temperature [1, 2]. Previous studies have also indicated that 5-HT can form highly ordered structures in a faulty oxidative environment and thus cause some types of mental disorders including schizophrenia, depression, and Alzheimer's disease [3, 4]. 5-HT is electroactive and thus the rapid electroanalysis of 5-HT has attracted much attention to date [5]. The oxidation mechanism of 5-HT is complicated, and the oxidation products involve oxidized dihydroxyindoles, dimers and polymers, depending on the experimental conditions [6-9]. However, to our knowledge, the oxidative polymerization of 5-HT to develop a biomacromolecule-immobilization matrix for biosensing applications has not been reported to date. In contrast, the polymerization of some other monoamine neurotransmitters such as dopamine and L-DOPA have been widely used in diverse areas including immobilization of biomacromolecules [10, 11], modification of surfaces [12], and environment analysis [13, 14], since the inception of intriguing polydopamine material about 10 years ago [15, 16]. Accordingly, the oxidative polymerization of 5-HT to develop new functional biocomposites is an interesting topic, which can enrich the family of monoamine neurotransmitter polymers for diverse potential applications including biosensing. In addition, compared with other monoamine neurotransmitter polymers, poly(5-HT) features its abundant amino groups for chemical modification in various promising applications.

Due to the necessity of daily check of the blood glucose level for millions of diabetics, glucose has become one of the most important analytes [17-19]. The nonenzymatic and enzymatic electroanalysis methods have been employed to quickly and sensitively analyze glucose [20]. The enzymatic method features excellent selectivity, and glucose oxidase (GOx) is often used for amperometric biosensing of glucose. Highly efficient immobilization of GOx by appropriate physical and chemical methods is the key step for electrochemical glucose biosensing [21, 22]. Many natural and artificial polymers have been examined as enzyme-immobilization matrixes, including natural biopolymer chitosan (CS) and

some monoamine neurotransmitter polymers like polydopamine (PDA) and poly(L-DOPA) (PD) [23, 24]. In our opinion, innovating polymer matrixes from chemical and biological reactions of biogenic molecules for high-load and high-activity immobilization of enzymes is always an intriguing theme for developing biosensors (and bioreactors) and even advancing bionic chemistry. Amperometric enzyme electrodes can also be used to fabricate enzymatic biofuel cells (BFCs), which are capable of harvesting electricity from oxidation of biofuels using enzymes as the catalysts [25, 26]. In recent years, GOx-based BFCs have received great attention because of their application potential in developing self-powered glucose sensors and even implantable devices [27-29].

Herein, a GOx-poly(5-HT)-Pd nanoparticles (PdNPs) bionanocomposite was synthesized through oxidative polymerization of 5-HT by Na_2PdCl_4 in GOx-containing neutral aqueous solution, and cast-coating the bionanocomposite and then CS on a Pd-plated Au electrode surface yields an enzyme electrode. The enzyme electrode exhibits good amperometric and BFC-based biosensing performance under optimized conditions. In addition to the physical entrapment of GOx, the covalent bonding of GOx on poly(5-HT) backbone via the amino chemistry of poly(5-HT) is experimentally proven (physical and chemical dual-immobilization for enzyme).

2. Experimental section

2.1. Instruments and reagents

All electrochemical experiments were carried out on a CHI660A electrochemical workstation (CH Instrument Co.). A conventional three-electrode electrolytic cell was employed. The working electrode was either an Au disk electrode with 2.0 mm diameter (area = 0.034 cm^2) or its modified electrodes, the reference electrode was a KCl-saturated calomel electrode (SCE), and the counter electrode was a graphite rod. All potentials here are reported with respect to SCE. An Autolab PGSTA 30 electrochemical workstation with an electrochemical noise module (Eco Chemie BV, the Netherlands) was used in the BFC experiments [30]. We employed a computer-interfaced HP4395A impedance analyzer and AT-cut 9 MHz gold-coated piezoelectric quartz crystals (6.0 mm diameter Au electrode, 12.5 mm diameter quartz wafer, keyhole configuration, Model JA5, Beijing Chenjing Electronics Co.,

Ltd., China) in the EQCM experiments [21]. UV-vis absorption spectra were recorded on a UV2450 UV-vis spectrophotometer (Shimadzu Co., Japan). Scanning electron microscopy (SEM) and transmission electron microscope (TEM) images were performed on a Hitachi S4800 scanning electron microscope with a field emission electron gun and a JEM-2100F transmission electron microscope (Japan), respectively.

GOx (EC 1.1.3.4, type II from *Aspergillus niger*) was purchased from Sigma. 5-HT and DA were purchased from Shanghai Macklin Biochemical Co., Ltd. (Shanghai, China). L-DOPA was purchased from Aladdin. 1-Ethyl-3-(3-dimethylaminopropyl)-carbodiimide hydrochloride (EDC) and N-hydroxysulfosuccinimide (Sulfo-NHS) were purchased from Sigma-Aldrich. $PdCl_2$ was purchased from Tianjin Chemical Reagents Station (Tianjin, China), and Na_2PdCl_4 solution was prepared by adding 28.4 mg $PdCl_2$ and 18.7 mg NaCl into 8 mL pure water. CS, Nafion, glucose, ascorbic acid, and uric acid were purchased from Sinopharm Chemical Reagent Co., Ltd. (Shanghai, China). 0.30 wt% CS solution was prepared in 0.10 M acetate buffer (pH 5.4). 0.30 wt% Nafion solution was prepared in alcohol. Glucose stock solution was allowed to mutarotate overnight at room temperature before use. A 30 wt% H_2O_2 solution was purchased from Shanghai Taopu Chemical Factory, and a fresh H_2O_2 solution was daily prepared. *p*-Benzoquinone (BQ) was purchased from Suzhou Time-Chem Technologies Co., Ltd. (Suzhou, China). A phosphate buffer consisting of 0.10 M KH_2PO_4-K_2HPO_4 + 0.1 M K_2SO_4 (pH 7.0) served as the supporting electrolyte. Human serum samples were donated by Hunan Normal University Hospital. All other chemicals were of analytical grade or better quality and used as received. Milli-Q ultrapure water (Millipore, ≥18 MΩ cm) was used throughout. All experiments were performed at room temperature around 25 ^{o}C.

2.2. Preparation and measurements of biosensors

The preparation of biosensors is illustrated in Scheme 1. The bare Au disk electrode was pretreated according to the reported protocol [31, 32]. At first, one drop of fresh prepared concentrated H_2SO_4 + H_2O_2 (3:1, v/v) was placed on the Au disk electrode surface for 15 s, and the Au disk electrode was rinsed thoroughly with water and then dried with a stream of pure nitrogen. The treatment was repeated three times. Prior to the electrochemical experiments, the Au disk electrode was subjected to repeated

potential cycling (-0.35~1.5 V, 50 mV s^{-1}) in 0.10 M aqueous H_2SO_4 until the cyclic voltammogram indicating that a clean Au disk electrode surface was obtained. Then, Pd was electroplated on the treated bare Au disk electrode (Pd_{plate}/Au) in 0.10 M aqueous H_2SO_4 containing 5.0 mM $PdCl_2$, by multipotential-step electrolysis from 1.1 to 0 V vs. SCE with a pulse width of 0.25 s, and the total time for the electrodeposition experiment was 400 s. The Pd_{plate}/Au electrode can excellently catalyze the electrooxidation of H_2O_2, as shown in Fig. S1. Then, a stirred phosphate buffer containing 40 mM 5-HT and 2.5 mg mL^{-1} GOx was subjected to chemical oxidative polymerization by adding 2.5 mM Na_2PdCl_4. The precipitation was observed in several min, and the reaction was allowed to occur for 2 h to maximize the formation of GOx-poly(5-HT)-PdNPs precipitate. Then, the biosensor was fabricated by coating Pd_{plate}/Au electrode with the GOx-poly(5-HT)-PdNPs bionanocomposite (2.5 μL) and then strengthening the enzyme film with CS (0.3 wt%, 1.5 μL) (CS/GOx-poly(5-HT)-PdNPs/Pd_{plate}/Au). CS is also well known as a good binder of high biocompatibility for enzyme immobilization. For comparison, CS/GOx-PDA-PdNPs/Pd_{plate}/Au, CS/GOx-PD-PdNPs/Pd_{plate}/Au, CS/GOx-polyaniline (PANI)-PdNPs/Pd_{plate}/Au, GOx-poly(5-HT)-PdNPs/Pd_{plate}/Au, CS/GOx-PdNPs/Pd_{plate}/Au, CS/GOx/Pd_{plate}/Au, and Nafion/GOx/Pd_{plate}/Au electrodes were similarly prepared, except for the use of DA, L-DOPA or aniline instead of 5-HT. When not in use, the prepared enzyme electrodes were stored in phosphate buffer at 4 ^oC (refrigerator). The EQCM Au electrode was cleaned as reported before [33]. Briefly, one drop of concentrated HNO_3 was placed on the EQCM electrode surface for 15 s, the follow-up procedures including electrode-modifications as required were the same as those for the above Au disk electrode.

In the first-generation biosensing mode, to detect the oxidation of enzymatically generated H_2O_2, the prepared enzyme electrodes were measured by potentiostating them at 0.7 V vs. SCE under solution-stirred conditions. The response current was recorded as the change value between the steady-state current after adding substrate and the initial background current without substrate. The clear liquid serum samples without further pretreatments were utilized for practical sample analysis [34, 35]. In the second-generation biosensing mode, the enzyme electrodes were tested by cyclic voltammetry (CV) in N_2-saturated quiescent phosphate buffer containing artificial mediator.

The BFC for self-powered glucose biosensing was fabricated as illustrated in Scheme S1. The anode compartment contained the CS/GOx-poly(5-HT)-PdNPs/Pd_{plate}/Au electrode in 20 mL of 0.1 M phosphate buffer (pH 7.0) containing 4.0 mM BQ and glucose at a specified concentration, and the cathode compartment, separated from the anode compartment by a Nafion 117 ion-exchange membrane, contained a Pd_{plate}/Au electrode in 0.40 M $KMnO_4$ + 0.50 M H_2SO_4 aqueous solution [36]. When the external resistance load was 1 kΩ, the BFC current developed between the two electrodes increased with the glucose concentration, in the absence of any external power source (i.e. self-powered biosensing).

2.3. Computational details

The possible polymerization sites of 5-HT are discussed by density function theory (DFT) calculations using the M062X function [37], as implemented in the Gaussian 09 program [38], using the standard Pople 6-31+g (d, p) basis set [39]. Wavefunctions are obtained in the ground state using DFT calculations with the M062X function with the 6-311+g (d, p) basis set [40]. The analysis of Fukui function and electrostatic potentials (ESP) on molecular van der Waals (vdW) surface is done using Multiwfn program [41, 42].

3. Results and discussion

3.1. Oxidative polymerization of 5-HT for preparing the enzyme electrodes

Some noble metal nanoparticles exhibit high electrocatalytic activity for oxidation of H_2O_2 and preparation of oxidase-based enzyme electrodes [43]. Here, electroplated Pd, Pt and Au on gold electrodes were examined, as shown in Fig. S1. The sensing current based on the anodic oxidation of H_2O_2 followed the order of Pt_{plate}/Au ≈ Pd_{plate}/Au > Au_{plate}/Au > bare Au electrode. Pd plating is selected here, because Pd behaves well as Pt but the use of Pd is obviously more environment-friendly due to the higher abundance of Pd on the earth than that of Pt [44, 45].

As stated before, Na_2PdCl_4 oxidized 5-HT in the aqueous solution containing GOx, and an insoluble GOx-poly(5-HT)-PdNPs bionanocomposite was obtained. UV-vis spectrophotometry was done to

examine the reactions, as shown in Fig. 1. Here, all solutions were prepared with phosphate buffer (0.1 M, pH 7.0), and the phosphate buffer was also used as a reference solution in the UV-vis spectrophotometry. 2.5 mM Na_2PdCl_4 solution showed an absorption band at 425 nm [46], the solution of 40 mM 5-HT was almost colorless, and 2.5 mg mL^{-1} GOx solution gave a yellow color. Fig. 1b shows the characteristic peaks of GOx at 276, 380 and 451 nm [47, 48]. The mixtures of 40 mM 5-HT + 2.5 mM Na_2PdCl_4, and 40 mM 5-HT + 2.5 mM Na_2PdCl_4 + 2.5 mg mL^{-1} GOx (2.5 mM Na_2PdCl_4 was finally added for each) was gold-yellow in color at first, after 30 min reaction and then 8 min centrifugation at 3500 rpm, we obtained yellow supernatants and insoluble poly(5-HT)-PdNPs and GOx-poly(5-HT)-PdNPs bionanocomposites at the bottom, respectively. Prior to subsequent experiments, centrifugation was repeatedly done until the supernatant was colorless. The formation of insoluble bionanocomposites implies the oxidation polymerization of 5-HT by Na_2PdCl_4, with simultaneous formation of PdNPs. In fact, a precipitate could also be formed after two days in air-saturated 100 mM tris-HCl buffer containing 40 mM 5-HT (pH 8.5), and a thin film of the precipitate could be robustly attached to the tagboard surface, as displayed in Fig. S2, implying that the self-polymerization of 5-HT after oxidation of 5-HT by oxygen in air is possible.

Obviously, electrochemistry methods are very useful for studying the oxidative polymerization mechanism of various monomers since the oxidation degrees of monomers, oligomers and polymers can be conveniently controlled and the electron-transfer reactions can be readily probed by the real-time electrochemical responses. The electrochemical oxidation and polymerization of 5-HT was investigated by CV in 0.1 M phosphate buffer (pH 7.0) containing 5-HT at several concentrations, as shown in Fig. 2. For 20 μM 5-HT, a cathodic current ramp due to the irreversible reduction of the soluble oxygen was observed at potentials negative to ca. -0.4 V, since this cathodic current ramp was also observed in the 5-HT-free blank solution and became notably smaller after nitrogen saturation of the solution (not shown). A small anodic shoulder peak due to oxidation of 5-HT was observed at ca. 0.4 V, which can be ascribed to the oxidation of phenolic hydroxyl and indole groups [49]. An anodic ramp due to the oxidation of Au was observed at potentials positive of ca. 0.5 V, since we observed a pair of redox peaks due to oxidation of Au (peaking at ca. 0.87 V) and reduction of Au oxides (at ca. 0.36 V) in the blank solution (not shown). After the anodic oxidation of 5-HT, a pair of small redox peaks centering at

ca. -0.14 V was observed, and their peak heights increased cycle by cycle, which can be attributed to the quinone/hydroquinone couple of the anodically formed dihydroxyindole [50]. With the increase of 5-HT concentration from 20 μM to 0.1 mM, 1 mM, and finally 40 mM, the anodic peak at ca. 0.4 V increased notably while the redox peaks at ca. -0.14 V increased much slowly, implying the synchronous occurrence of competitive deep-oxidation reactions of 5-HT at high concentrations, such as oligomerization and polymerization [50]. The 5-HT-oxidation peak at ca. 0.4 V also notably decreased cycle by cycle for each 5-HT concentration (except for the very small oxidation peak of 20 μM 5-HT), and such peak decrease from the first cycle to the second cycle was the most significant for 40 mM 5-HT, indicating the most significant electrodeposition of electron-insulating polymer during the first-cycle oxidation of 40 mM 5-HT against the second-cycle electrooxidation of 5-HT here. These Au electrodes after experiencing 5-HT oxidation were characterized by CV and electrochemical impedance spectroscopy of the $Fe(CN)_6^{3-/4-}$ probe [30], as shown in Fig. S3 with discussion detailed. Both CV and electrochemical impedance spectroscopy (EIS) characterizations revealed that the reversibility of the $Fe(CN)_6^{3-/4-}$ probe was decreased with the increase of 5-HT concentration, demonstrating that electrooxidation of 5-HT at a higher concentration can increase the quantity of electron-insulating poly(5-HT) on the Au electrode. From the above experiments/discussion and the well-known mechanism for a general polymerization process, we believe that the oxidation of 5-HT is a complicated multistep process. At very low concentrations, oxidation of 5-HT may produce a dihydroxyindole derivative as the main product [50], and the chemical bonding between 5-HT molecules for chain propagation is very difficult due to the very small probability of mutual collisions of 5-HT molecules at very low concentrations. At medium concentrations with increased probability of mutual collisions of 5-HT molecules, oxidation of 5-HT may produce dimers, oligomers, polymer, and the dihydroxyindole derivative [51]. At high concentrations, oxidation of the crowded 5-HT molecules allows chain propagation for polymerization of 5-HT, in addition to the limited formation of dimers, oligomers, and the dihydroxyindole derivative. Furthermore, the EQCM technique was used to track the electropolymerization process of 40 mM 5-HT in 0.1 M phosphate buffer (pH 7.0). Fig. S4 shows the EQCM responses to CV electropolymerization of 5-HT in 0.1 M phosphate buffer (pH 7.0) containing

40 mM 5-HT. An anodic current peak for 5-HT oxidation was observed at ca. 0.4 V vs. SCE in the first positive scan, accompanying with a notable frequency decrease. The total net frequency decrease ($-\Delta f_0$) was 566 Hz after 20 potential cycles. All current peaks and the resonant frequency decreased with the progress of potential cycling, proving the continuous electrochemical formation of electron-insulating poly(5-HT) deposit on the electrode.

To gain further insights into the origin of the reaction mechanism of 5-HT, we have calculated the Fukui function to evaluate their ability for the electrophilic attack and nucleophilic attack (Fig. S5, Fig. S6 and Table S1) [52]. Clearly, most positive parts of f^- function are localized in N13, C6, C7, C3, O24, C5, C8, and C4, which means the positions of (C6，C5) , (C7, C8) and (C3, C4) are favorite reactive sites for electrophilic attack or free radical attack. Although almost identical positive parts of f^- function are localized in N13 and O24, the N13 and the O24 are not vulnerable sites for electrophilic attack since both nitrogen and oxygen possess readily polarized lone pair electrons. In addition, most positive parts of f^+ function are localized in H14, H12, H19, H23, H9, H20, and H22, indicating that these positions are favorite reactive sites for nucleophilic attack. At the same time, we suspect that H25 is also vulnerable to nucleophilic attacks. To further confirm this, ESP on 5-HT molecule vdW surface is analyzed [53]. As shown in Fig. S6, a local surface maximum value (48.99 kcal/mol) near H25 is shown, suggesting that the electron density is locally depleted and H25 is also a highly vulnerable site for nucleophilic attack.

According to the above findings and the reported polymerization mechanisms for indole and dopamine of similar chemical structures [16, 54, 55], as well as the oxidation mechanism reported for 5-HT (Scheme S2) [50, 56], we believe that the oxidative polymerization mechanism of 5-HT is the indole-like polymerization through chain propagation mainly at 1, 2, 4, 6, and 7 sites (Scheme S3). Anyway, the exact oxidative polymerization mechanism of 5-HT is very complicated due to the presence of several possible active sites in the 5-HT molecule for chain propagation, and thus more in-depth studies are required to clarify the exact chemical structure of poly(5-HT).

SEM images displayed in Fig. 3 reveal the surface morphology of Au disk electrode and its modified electrodes. The bare Au disk electrode (a) displays a rather smooth surface. Many aggregated Pd

nanoparticles (ca. 100 nm) are clearly seen at Pd_{plate}/Au electrode (b). After cast-coating the GOx-poly(5-HT)-PdNPs bionanocomposite on the Pd_{plate}/Au disk electrode (c), a blanket of aggregated nanoparticles is clearly seen. After further cast-coating of CS (d), the outer surface is newly covered with a glue-like film. The TEM image of the GOx-poly(5-HT)-PdNPs bionanocomposite is displayed in Fig. 3 (e), which proves the formation of Pd nanoparticles with a statistically dominant size of 3 nm and confirms the fact that Na_2PdCl_4 can oxidize 5-HT in the aqueous solution containing GOx to produce PdNPs. Furthermore, the electrode modification was characterized by CV and EIS of the $Fe(CN)_6^{3-/4-}$ probe (Fig. S7 with discussion detailed), both implying that the enzyme film has been successfully constructed on Au electrode surface.

3.2. Mass-specific activity of immobilized GOx and biosensing performance of the enzyme electrode

The amperometric method was used to estimate the mass-specific activity of native or immobilized GOx in pH 7.0 phosphate buffer containing either GOx or GOx-poly(5-HT)-PdNPs dispersion, as shown in Fig. S8. One unit of GOx activity (U) is defined here as the production of 1 μmol H_2O_2 in 60 s under our experimental conditions. The enzymatic specific activity (ESA) can be written as $\mathrm{ESA} = n_{H_2O_2} / \Delta m_{GOx}$, where $n_{H_2O_2}$ in μmol is the molar quantity of H_2O_2 produced in the 60 s enzymatic reaction obtained from amperometric standard curve method under our experimental conditions, and Δm_{GOx} is the added mass of native and immobilized GOx. Such an amperometric method to estimate the ESA values has been proposed and discussed in detail in our previous reports [57-60]. Here, the mass of added GOx (Δm_{GOx}) for native GOx and immobilized GOx (entrapped in the GOx-poly(5-HT)-PdNPs bionanocomposite) were both 12.5 μg. We obtained the current change value on the Au disk electrode at 0.7 V vs. SCE in the sequent 60 s as 1.12 μA and 1.05 μA for native and immobilized GOx, respectively. Hence, $n_{H_2O_2}$ is calculated according to the calibration curve (Fig. S8A) to be 0.85 μmol for native GOx and 0.80 μmol for immobilized GOx. The ESA values of native and immobilized GOx were measured to be 68 kU g^{-1} and 64 kU g^{-1}, respectively. Thus, the enzymatic relative activity ($\mathrm{ERA} = \mathrm{ESA_i}/\mathrm{ESA_n}$) is estimated to be 94.1%. For comparison, we also estimated the

mass-specific activities of the immobilized GOx in the PDA and PD cases under identical conditions, the enzymatic relative activity are estimated as 80% and 65%, respectively (Fig. S8), quantitatively demonstrating that the proposed enzyme-immobilization protocol based on the poly(5-HT) matrix is indeed promising for preservation of the higher activity of enzyme.

To obtain the best sensitivity for glucose assay, various experimental conditions, including the concentration of GOx, 5-HT and Na_2PdCl_4, the volume of CS, and detection potential and pH value were investigated by varying the examined parameter while others were fixed, as shown in Fig. S9 with discussion detailed. The optimized conditions for enzyme electrode fabrication are 40 mM 5-HT, 2.5 mg mL^{-1} GOx, 2.5 mM Na_2PdCl_4, and 1.5 μL 0.30 wt% CS, and the optimized parameters for biosensing experiments are pH 7.0 phosphate buffer and test potential at 0.70 V vs. SCE.

The performance of the biosensor in the first-generation biosensing mode was tested. Under optimized conditions, the amperometric glucose-biosensing responses (A) and the calibration curves (B) of several enzyme electrodes are displayed in Fig. 4. The amperometric response to glucose reaches steady-state within ca. 5 s in each case. The response at the CS/GOx-poly(5-HT)-PdNPs/Pd_{plate}/Au electrode is linear with glucose concentration from 2.0 μM to 6.66 mM (R^2= 0.993), with a sensitivity of 110 μA mM^{-1} cm^{-2} and a LOD (S/N=3) of 0.2 μM. The sensitivity is superior to CS/GOx-PDA-PdNPs/Au (87.2 μA mM^{-1} cm^{-2}), CS/GOx-PD-PdNPs/Au (55.3 μA mM^{-1} cm^{-2}), CS/GOx-PANI-PdNPs/Pd_{plate}/Au (10.7 μA mM^{-1} cm^{-2}), CS/GOx/Pd_{plate}/Au (61.0 μA mM^{-1} cm^{-2}), Nafion/GOx/Pd_{plate}/Au (58.4 μA mM^{-1} cm^{-2}) , CS/GOx-Na_2PdCl_4/Pd_{plate}/Au (2.35 μA mM^{-1} cm^{-2}) and many reported GOx electrodes (Table S2). However, the sensitivity is slightly worse than GOx-poly(5-HT)-PdNPs/Pd_{plate}/Au (126 μA mM^{-1} cm^{-2}) electrode, but the GOx-poly(5-HT)-PdNPs/Pd_{plate}/Au electrode has a poorer stability probably due to the shedding of enzymes (Fig. S10). From the above data, we conclude that poly(5-HT) is an excellent polymer matrix to entrap GOx for amperometric biosensing under the examined conditions.

The apparent Michaelis-Menten constant (K_m^{app}) is an indicator of the enzyme-substrate kinetics. According to the Lineweaver-Burk equation [36], K_m^{app} is obtained as 4.07 mM at CS/GOx-poly(5-HT)-PdNPs/Pd_{plate}/Au electrode, as also shown in Fig. 4. The estimated K_m^{app} is lower

than the reported value of 15.2 mM for the GOx immobilized at the boron-doped carbon nanotubes and many others [61-63], implying that the immobilized GOx has high bioactivity and affinity to glucose.

The anti-interference ability, reproducibility and storage stability of the biosensor were investigated by amperometric measurements. As shown in Fig. S11, the additions of 0.1 mM ascorbic acid and uric acid caused very small interference to the determination of glucose, and the interfering signal is increased with the concentration as expected. The reproducibility of this biosensor was evaluated with a relative standard deviation of 2.3% (n=5) for 1 mM glucose, and our amperometric enzyme electrode maintained 95% of its initial current response after 20 days (Fig. S11). The biosensor was used for practical analysis in several human serum samples. Serum sample (0.1 mL) was added to 10 mL phosphate buffer (0.1 M, pH 7.0) as testing solution and a potential of 0.7 V vs. SCE was applied. The concentrations of glucose in serum is calculated from the calibration curve, and the values measured at CS/GOx-poly(5-HT)-PdNPs/Pd_{plate}/Au electrode agree well with the hospital results (Table S3). The satisfactory results originate mainly from the facts that GOx is highly specific to glucose and the high sensitivity of our enzyme electrode allows a high-ratio sample-solution-dilution that can minimize the background and interferences.

The concentration of dissolved O_2 in aqueous solutions is only ca. 1 mM, which limits the linear detection range (LDR) of the first generation biosensor. Hence, our amperometric enzyme electrode was also exploited to determine glucose in the second-generation biosensing mode with the solution-state redox mediators of BQ. As shown in Fig. 5, in the presence of 4 mM BQ, we observed a pair of well-defined redox peaks of BQ, centering at ca. 0.2 V vs. SCE on the CS/GOx-poly(5-HT)-PdNPs/Pd_{plate}/Au electrode, and the anodic peak was notably increased while the cathodic peak was decreased with the increase of BQ concentration. The LDR was favorably extended to 40 mM glucose with a slope of 71.0 μA mM^{-1} cm^{-2}. The above results demonstrate that the biosensor can evolve into a second-generation biosensor with a wider LDR by simple addition of a redox mediator in the detection solution.

In addition, a monopolar BFC was constructed using our enzyme electrode as the anode for glucose oxidation and a Pd_{plate}/Au electrode as the cathode for $KMnO_4$ reduction. As shown in Fig. 6, the BFC exhibited an open-circuit potential of 1.0 V, a short-circuit current of 4.24 mA cm^{-2}, and a maximum

power density (P_{max}) of 2.31 mW cm^{-2}. This P_{max} is much larger than most reported values [36, 64], indicating that the enzyme film is an excellent anodic material for BFC development. As shown in Fig. 6, the BFC as a self-powered glucose sensor exhibited a linear relationship to glucose concentration from 50 μM to 34.5 mM with a sensitivity of 71.7 μA mM^{-1} cm^{-2}, which effectively broadens the linear range of glucose detection versus the first-generation amperometric biosensing mode.

3.3. Chemical immobilization of GOx based on the amino chemistry of poly(5-HT)

The enzyme-immobilization protocol presented above is based on the physical entrapment principle. In fact, poly(5-HT) is an amino-rich polymer, and thus the high reactivity of the pending amino groups can be exploited for chemical immobilization of enzyme molecules. Such a combined physical and chemical protocol for enzyme immobilization seems to be of sufficient novelty and significance in the area of enzyme electrode including the application for glucose detection. Herein, the electrochemical and chemical polymerization of 5-HT was employed for preliminary principle validation of the idea of physical and chemical dual-immobilization of enzyme.

First, one-step electrochemical codeposition of poly(5-HT), GOx and Na_2PdCl_4 by CV was conducted on Pd_{plate}/Au electrode in 0.1 M phosphate buffer (pH 7.0) containing 40 mM 5-HT, 2.5 mg mL^{-1} GOx and 2.5 mM Na_2PdCl_4 under stirring condition (to maximally homogenize this precipitation mixture), yielding a poly(5-HT)-GOx-PdNPs/Pd_{plate}/Au electrode. Then, 2.5 μL aqueous solution containing 10 mg mL^{-1} GOx, 20 mM EDC, and 5 mM NHS was cast-coated on the above electrode (GOx_{chem}/poly(5-HT)-GOx-PdNPs/Pd_{plate}/Au). Fig. 7A shows the amperometric responses to glucose at poly(5-HT)-GOx-PdNPs/Pd_{plate}/Au and GOx_{chem}/poly(5-HT)-GOx-PdNPs/Pd_{plate}/Au electrodes under optimized conditions. The sensitivity at GOx_{chem}/poly(5-HT)-GOx-PdNPs/Pd_{plate}/Au electrode is ca. 1.56 fold that at poly(5-HT)-GOx-PdNPs/Pd_{plate}/Au, demonstrating that the amino chemistry of poly(5-HT) can indeed be used for further chemical tethering of GOx molecules and the idea of physical and chemical dual-immobilization of enzyme is thus supported. Furthermore, poly(5-HT)-GOx/Pd_{plate}/Au and GOx_{chem}/poly(5-HT)-GOx/Pd_{plate}/Au electrodes were similarly prepared without Na_2PdCl_4, the sensitivity at GOx_{chem}/poly(5-HT)-GOx/Pd_{plate}/Au electrode is ca. 1.62 fold that

at poly(5-HT)-GOx/Pd_{plate}/Au electrode (Fig. S12A). For comparison, GOx/poly(5-HT)-GOx-PdNPs/Pd_{plate}/Au were similarly prepared without crosslinking agent (EDC/NHS) (Fig. S13), and we found that the sensitivity at GOx/poly(5-HT)-GOx/Pd_{plate}/Au electrode is almost the same as that at poly(5-HT)-GOx/Pd_{plate}/Au electrode, demonstrating that the further chemical tethering of GOx on poly(5-HT) molecules cannot be achieved without crosslinking agent (EDC/NHS). PDA-GOx/Pd_{plate}/Au and GOx_{chem}/PDA-GOx/Pd_{plate}/Au electrodes were also similarly prepared, except for the use of DA instead of 5-HT. The sensitivity at GOx_{chem}/PDA-GOx/Pd_{plate}/Au electrode is only ca. 1.04 fold that at PDA-GOx/Pd_{plate}/Au electrode (Fig. S12B), demonstrating that PDA is lack of amino groups and thus a further chemical tethering of GOx molecules via the amino chemistry is very small. It should be noted that the amperometric responses here in the electropolymerization case are notably lower than the counterparts in the chemopolymerization case as before, probably due to the limited load and activity of the electropolymerization-entrapped enzyme, as reported in our previous study [21].

Second, the prepared GOx-poly(5-HT)-PdNPs suspension was centrifuged (three times, 3000 rpm, 5 min) and then redispersed in the phosphate buffer. 2.5 μL redispersed precipitate was cast-coated on the Pd_{plate}/Au electrode, yielding a poly(5-HT)-GOx-PdNPs/Pd_{plate}/Au electrode. Then, 2.5 μL aqueous solution containing 8 mg mL^{-1} GOx, 20 mM EDC, and 5 mM NHS was cast-coated on the above electrode, and the reaction was allowed to occur for 5 h at room temperature. Finally, 1.5 μL of 0.3 wt% CS solution was cast-coated to strengthen the enzyme film. The prepared electrode is denoted as CS/GOx_{chem}/poly(5-HT)-GOx-PdNPs/Pd_{plate}/Au electrode. As shown in Fig. 7B, the sensitivity at CS/GOx_{chem}/poly(5-HT)-GOx-PdNPs/Pd_{plate}/Au electrode is ca. 1.42 fold that at CS/poly(5-HT)-GOx-PdNPs/Pd_{plate}/Au electrode. For comparison, a CS/GOx_{chem}/PDA-GOx-PdNPs/Pd_{plate}/Au electrode was prepared by the same process. The sensitivity at the CS/GOx_{chem}/PDA-GOx-PdNPs/Pd_{plate}/Au electrode is only ca. 1.06 fold that at CS/PDA-GOx-PdNPs/Pd_{plate}/Au electrode, as shown in Fig. S14. From the above data, it can be concluded that poly(5-HT) possesses much more abundant amino groups than PDA, and thus this unique structural characteristic enables convenient physical and chemical dual-immobilization of enzyme and other biomacromolecules for wider potential applications including the detection of

glucose.

4. Conclusions

In summary, a novel enzyme electrode has been constructed based on the oxidative polymerization of 5-HT by Na_2PdCl_4 in GOx-containing neutral aqueous solution to immobilize GOx. The thus-prepared enzyme biosensor exhibits higher sensitivity and lower LOD, in comparison with enzyme-immobilization polymer matrixes of PD, PDA, PANI, and/or common CS and Nafion. Also, the enzymatic relative activity of GOx immobilized in poly(5-HT) is better than those in the PDA and PD cases. Our study also suggests that the thus-fabricated BFC device can be applied as a self-powered biosensor for glucose analysis with a wide linear detection range. Poly(5-HT) as an amino-rich polymer is facile for amino-based chemical modification, including the physical and chemical dual-immobilization of enzyme tentatively discussed here, and more relevant researches on poly(5-HT) are in progress in this laboratory.

Acknowledgments

This work was supported by the National Natural Science Foundation of China (21475041, 21675050, 20405142, 21305041), Hunan Lotus Scholars Program (2011), and Foundations of the Education Department and the Science & Technology Department of Hunan Province (14C0712, 2016SK2020).

References

[1] P. Hashemi, E. C. Dankoski, J. Petrovic, R. B. Keithley, R. M. Wightman, Voltammetric detection of 5-hydroxytryptamine release in the rat brain, Anal. Chem. 81 (2009) 9462-9471.

[2] M. Labib, E. H. Sargent, S. O. Kelley, Electrochemical methods for the analysis of clinically relevant biomolecules, Chem. Rev. 116 (2016) 9001-9090.

[3] D. E. Nichols, C. D. Nichols, Serotonin receptors, Chem. Rev. 108 (2008) 1614-1641.

[4] S. Claeysen, J. l. Bockaert, P. Giannoni, Serotonin: a new hope in Alzheimer's disease?, ACS Chem. Neurosci. 6 (2015) 940-943.

[5] Y. Wang, W. Shi, T. Li, Q. Min, X. Jin, Q. Wang, J. Xie, Y. Yuan, S. Wu, X. Li, A disposable electrochemical sensor for simultaneous determination of norepinephrine and serotonin in rat cerebrospinal fluid based on mwnts-zno/chitosan composites modified screen-printed electrode, Biosens. Bioelectron. 65 (2014) 31–38.

[6] M. C. Henstridge, G. G. Wildgoose, R. G. Compton, Generator/collector experiments with a single electrode: introduction and application to exploring the oxidation mechanism of serotonin, J. Phys. Chem. C 113 (2009) 14285-14289.

[7] P. Shi, X. Miao, Y. Hong, S. Lin, B. Wei, J. Chen, X. Lin, Y. Tang, Characterization of poly(5-hydroxytryptamine)-modified glassy carbon electrode and applications to sensing of norepinephrine and uric acid in preparations and human urines, Electrochim. Acta 92 (2013) 341-348.

[8] M. Z. Wrona, G. Dryhurst, Oxidations chemistry of 5-hat. 1. mechanism and products pormed at micromolar concentrations, J. Org. Chem. 52 (1987) 2817-2825.

[9] M. Z. Wrona, G. Dryhurst, Oxidation of serotonin by superoxide radical: implications to neurodegenerative brain disorders, Chem. Res. Toxicol. 11 (1998) 639-650.

[10] M. Dai, L. Sun, L. Chao, Y. Tan, Y. Fu, C. Chen, Q. Xie, Immobilization of enzymes by electrochemical and chemical oxidative polymerization of L-DOPA to fabricate amperometric biosensors and biofuel cells, ACS Appl. Mater. Interfaces 7 (2015) 10843-10852.

[11] Y. Fu, P. Li, Q. Xie, X. Xu, L. Lei, C. Chao, C. Zou, W. Deng, S. Yao, One-pot preparation of polymer–enzyme–metallic nanoparticle composite films for high-performance biosensing of glucose and galactose, Adv. Funct. Mater. 19 (2009) 1784-1791.

[12] R. Sa, Y. Yan, Z. Wei, L. Zhang, W. Wang, M. Tian, Surface modification of aramid fibers by bio-inspired poly (dopamine) and epoxy functionalized silane grafting, ACS Appl. Mater. Interfaces 6 (2014) 21730-21738.

[13] J. Kim, B. Raman, K. H. Ahn, Artificial receptors that provides a preorganized hydrophobic environment: a

biomimetic approach to dopamine recognition in water, J. Org. Chem. 71 (2006) 38-45.

[14] Q. Song, M. Li, H. Li, Q. Wu, Y. Zhou, Y. Wang, Bifunctional polydopamine@Fe_3O_4 core–shell nanoparticles for electrochemical determination of lead(II) and cadmium(II), Anal. Chim. Acta 787 (2013) 64-70.

[15] H. Lee, S. M. Dellatore, W. M. Miller, P. B. Messersmith, Messersmith, P. B., mussel-inspired surface chemistry for multifunctional coatings, Science 318 (2007) 426-430.

[16] Y. Li, M. Liu, C. Xiang, Q. Xie, S. Yao, Electrochemical quartz crystal microbalance study on growth and property of the polymer deposit at gold electrodes during oxidation of dopamine in aqueous solutions, Thin Solid Films 497 (2006) 270-278.

[17] S. Ina, K. Ninomiya, T. Mogi, A. Hase, T. Ando, N. Matsukaze, J. Ogihara, M. Akao, H. Kumagai, H. Kumagai, Rice (*oryza sativa japonica*) albumin suppresses the elevation of blood glucose and plasma insulin levels after oral glucose loading, J. Agric. Food Chem. 64 (2016) 4882-4890.

[18] B. Liu, Z. Sun, P. J. Huang, J. Liu, Hydrogen peroxide displacing DNA from nanoceria: mechanism and detection of glucose in serum, J. Am. Chem. Soc. 137 (2015) 1290-1295.

[19] C. Sun, X. Chen, Q. Han, M. Zhou, C. Mao, Q. Zhu, J. Shen, Fabrication of glucose biosensor for whole blood based on Au/hyperbranched polyester nanoparticles multilayers by antibiofouling and self-assembly technique, Anal. Chim. Acta 776 (2013) 17-23.

[20] C. Chen, Q. Xie, D. Yang, H. Xiao, Y. Fu, Y. Tan, S. Yao, Recent advances in electrochemical glucose biosensors: a review, RSC Adv. 3 (2013) 4473-4491.

[21] Y. Fu, C. Chen, Q. Xie, X. Xu, C. Zou, Q. Zhou, L. Tan, H. Tang, Y. Zhang, S. Yao, Immobilization of enzymes through one-pot chemical preoxidation and electropolymerization of dithiols in enzyme-containing aqueous suspensions to develop biosensors with improved performance, Anal. Chem. 80 (2008) 5829-5838.

[22] Z. Yang, Y. Cao, J. Li, Z. Jian, Y. Zhang, X. Hu, Platinum nanoparticles functionalized nitrogen doped graphene platform for sensitive electrochemical glucose biosensing, Anal. Chim. Acta 871 (2015) 35-42.

[23] Y. Fu, P. Li, L. Bu, T. Wang, Q. Xie, X. Xu, L. Lei, C. Zou, S. Yao, Chemical/biochemical preparation of new polymeric bionanocomposites with enzyme labels immobilized at high load and activity for high-performance electrochemical immunoassay, J. Phys. Chem. C 114 (2010) 1472-1480.

[24] M. Dai, T. Huang, L. Chao, Q. Xie, Y. Tan, C. Chen, W. Meng, Horseradish peroxidase-catalyzed polymerization of L-DOPA for mono-/bi-enzyme immobilization and amperometric biosensing of H_2O_2 and uric acid, Talanta 149 (2016) 117-123.

[25] M. J. Moehlenbrock, R. L. Arechederra, K. H. Sjöholm, S. D. Minteer, Analytical techniques for

characterizing enzymatic biofuel cells, Anal. Chem. 81 (2009) 9538-9545.

[26] N. P. Godman, J. L. DeLuca, S. R. McCollum, D. W. Schmidtke, D. T. Glatzhofer, Electrochemical characterization of layer-by-layer assembled ferrocene-modified linear poly (ethylenimine)/enzyme bioanodes for glucose sensor and biofuel cell applications, Langmuir 32 (2016) 3541-3551.

[27] R. A. Blaik, E. Lan, H. Yu, B. Dunn, Gold-coated M13 bacteriophage as a template for glucose oxidase biofuel cells with direct electron transfer, Acs Nano 10 (2015) 324-332.

[28] E. Katz, O. Lioubashevski, I. Willner, Magnetic field effects on bioelectrocatalytic reactions of surface-confined enzyme systems: enhanced performance of biofuel cells, J. Am. Chem. Soc. 127 (2005) 3979-3988.

[29] K. P. Prasad, Y. Chen, P. Chen, Three-dimensional graphene-carbon nanotube hybrid for high-performance enzymatic biofuel cells, ACS Appl. Mater. Interfaces 6 (2014) 3387-3393.

[30] Y. Tan, Q. Xie, J. Huang, W. Duan, M. Ma, S. Yao, Study on glucose biofuel cells using an electrochemical noise device, Electroanalysis 20 (2008) 1599-1606.

[31] Y. Xiao, R. Y. Lai, K. W. Plaxco, Preparation of electrode-immobilized, redox-modified oligonucleotides for electrochemical DNA and aptamer-based sensing, Nat. Protoc. 2 (2007) 2875-2880.

[32] J. Zhang, S. Song, L. Wang, D. Pan, C. Fan, A gold nanoparticle-based chronocoulometric DNA sensor for amplified detection of DNA, Nat. Protoc. 2 (2007) 2888-2895.

[33] Q. Xie, C. Xiang, Y. Yuan, Y. Zhang, L. Nie, S. Yao, A novel dual-impedance-analysis EQCM system—investigation of bovine serum albumin adsorption on gold and platinum electrode surfaces, J. Colloid Interface Sci. 262 (2003) 107-115.

[34] V. Singh, C. Rodenbaugh, S. Krishnan, Magnetic optical microarray imager for diagnosing type of diabetes in clinical blood Serum Samples, ACS sensors 1 (2016) 437-443.

[35] Z. Yang, C. Zhang, J. Zhang, W. Bai, Potentiometric glucose biosensor based on core–shell Fe_3O_4–enzyme–polypyrrole nanoparticles, Biosens. Bioelectron. 51 (2014) 268-273.

[36] C. Chen, L. Wang, Y. Tan, C. Qin, F. Xie, Y. Fu, Q. Xie, J. Chen, S. Yao, High-performance amperometric biosensors and biofuel cell based on chitosan-strengthened cast thin films of chemically synthesized catecholamine polymers with glucose oxidase effectively entrapped, Biosens. Bioelectron. 26 (2011) 2311-2316.

[37] Y. Zhao, D. G. Truhlar, The M06 suite of density functionals for main group thermochemistry, thermochemical kinetics, noncovalent interactions, excited states, and transition elements: two new functionals and systematic testing of four M06-class functionals and 12 other functionals, Theor. Chem. Acc. 120 (2008)

215-241.

[38] M. J. Frisch, G. Trucks, H. Schlegel, G. Scuseria, M. Robb, J. Cheeseman, G. Scalmani, V. Barone, B. Mennucci, G. Petersson, Gaussian 09, revision A. 1, Gaussian Inc., Wallingford, CT (2009)

[39] P. C. Hariharan, J. A. Pople, The influence of polarization functions on molecular orbital hydrogenation energies, Theor. Chim. Acta 28 (1973) 213-222.

[40] R. Krishnan, J. S. Binkley, R. Seeger, J. A. Pople, Self-consistent molecular orbital methods. XX. A basis set for correlated wave functions, J. Chem. Phys. 72 (1980) 650-654.

[41] T. Lu, F. Chen, Multiwfn: a multifunctional wavefunction analyzer, J. Comput. Chem. 33 (2012) 580-592.

[42] T. Lu, F. Chen, Revealing the nature of intermolecular interaction and configurational preference of the nonpolar molecular dimers $(H_2)_2$, $(N_2)_2$, and $(H_2)(N_2)$, J. Mol. Model. 19 (2013) 5387-5395.

[43] A. Popa, E. C. Abenojar, A. Vianna, C. Y. Buenviaje, J. Yang, C. B. Pascual, A. C. S. Samia, Fabrication of metal nanoparticle-modified screen printed carbon electrodes for the evaluation of hydrogen peroxide content in teeth whitening strips, J. Chem. Educ. 92 (2015) 1913-1917.

[44] M. Shao, J. Odell, M. Humbert, T. Yu, Y. Xia, Electrocatalysis on shape-controlled palladium nanocrystals: oxygen reduction reaction and formic acid oxidation, J. Phys. Chem. C 117 (2013) 4172–4180.

[45] L. Sun, Y. Ma, Z. Pei, C. Long, T. Huang, Q. Xie, C. Chao, S. Yao, An amperometric enzyme electrode and its biofuel cell based on a glucose oxidase-poly(3-anilineboronic acid)-pd nanoparticles bionanocomposite for glucose biosensing, Talanta 138 (2015) 100-107.

[46] Y. M. Lu, H. Z. Zhu, W. G. Li, B. Hu, S. H. Yu, Size-controllable palladium nanoparticles immobilized on carbon nanospheres for nitroaromatic hydrogenation, J. Mater. Chem. A 1 (2013) 3783-3788.

[47] M. R. Guascito, D. Chirizzi, C. Malitesta, E. Mazzotta, Mediator-free amperometric glucose biosensor based on glucose oxidase entrapped in poly(vinyl alcohol) matrix, Analyst 136 (2011) 164-173.

[48] R. J. Chung, A. N. Wang, S. Y. Peng, An enzymatic glucose sensor composed of carbon-coated nano tin sulfide, Nanomaterials 7 (2017) 39-46.

[49] K. Dhanalakshmi, R. Saraswathi, Electrochemical preparation and characterization of conducting copolymers: poly(pyrrole-co-indole), J. Mater. Sci. 36 (2001) 4107-4115.

[50] B. V. Sarada, T. N. Rao, D. A. Tryk, A. Fujishima, Electrochemical oxidation of histamine and serotonin at highly boron-doped diamond electrodes, Anal. Chem. 72 (2000) 1632-1638.

[51] M. Z. Wrona, G. Dryhurst, Further insights into the oxidation chemistry of 5-hydroxytryptamine, J. Pharm. Sci. 77 (1988) 911-917.

[52] R. G. Parr, W. Yang, Density functional approach to the frontier-electron theory of chemical reactivity, J. Am. Chem. Soc. 106 (1984) 4049-4050.

[53] T. Lu, S. Manzetti, Wavefunction and reactivity study of benzo[a]pyrene diol epoxide and its enantiomeric forms, Struct. Chem. 25 (2014) 1521-1533.

[54] H. Talbi, G. Monard, M. Loos, D. Billaud, Theoretical study of indole polymerization, J. Mol. Struct.: theochem 434 (1998) 129–134.

[55] Y. Liu, K. Ai, L. Lu, Polydopamine and its derivative materials: synthesis and promising applications in energy, environmental, and biomedical fields, Chem. Rev. 114 (2014) 5057-5115.

[56] G. Dryhurst, Applications of electrochemistry in studies of the oxidation chemistry of central nervous system indoles, Chem. Rev. 90 (1990) 795-811.

[57] C. Chen, Y. Fu, C. Xiang, Q. Xie, Q. Zhang, Y. Su, L. Wang, S. Yao, Electropolymerization of preoxidized catecholamines on prussian blue matrix to immobilize glucose oxidase for sensitive amperometric biosensing Biosens. Bioelectron. 24 (2009) 2726-2729.

[58] W. Wang, C. Qin, Q. Xie, X. Qin, L. Chao, Y. Huang, M. Dai, C. Chen, J. Huang, J. Hu, Rapid electrodeposition of a gold–Prussian blue nanocomposite with ultrahigh electroactivity for dual-potential amperometric biosensing of uric acid, Analyst 139 (2014) 2904-2911.

[59] Y. Su, Q. Xie, C. Chen, Q. Zhang, M. Ma, S. Yao, Electrochemical quartz crystal microbalance studies on enzymatic specific activity and direct electrochemistry of immobilized glucose oxidase in the presence of sodium dodecyl benzene sulfonate and multiwalled carbon nanotubes, Biotechnol. Prog. 24 (2008) 262-272.

[60] C. Deng, M. Li, Q. Xie, M. Liu, Y. Tan, X. Xu, S. Yao, New glucose biosensor based on a poly(o -phenylendiamine)/glucose oxidase-glutaraldehyde/Prussian blue/Au electrode with QCM monitoring of various electrode-surface modifications, Anal. Chim. Acta 557 (2006) 85-94.

[61] X. Chen, J. Chen, C. Deng, C. Xiao, Y. Yang, Z. Nie, S. Yao, Amperometric glucose biosensor based on boron-doped carbon nanotubes modified electrode, Talanta 76 (2008) 763-767.

[62] X. Liu, L. Shi, W. Niu, H. Li, G. Xu, Amperometric glucose biosensor based on single-walled carbon nanohorns, Biosens. Bioelectron. 23 (2008) 1887-1890.

[63] Z. Zhang, Y. Xie, Z. Liu, F. Rong, Y. Wang, D. Fu, Covalently immobilized biosensor based on gold nanoparticles modified TiO_2 nanotube arrays, J. Electroanal. Chem. 650 (2011) 241-247.

[64] Q. Lang, Y. Long, J. Shi, L. Liang, X. Lin, A. Liu, Co-immobilization of glucoamylase and glucose oxidase for electrochemical sequential enzyme electrode for starch biosensor and biofuel cell, Biosens. Bioelectron. 51C

1 (2013) 158-163.

2

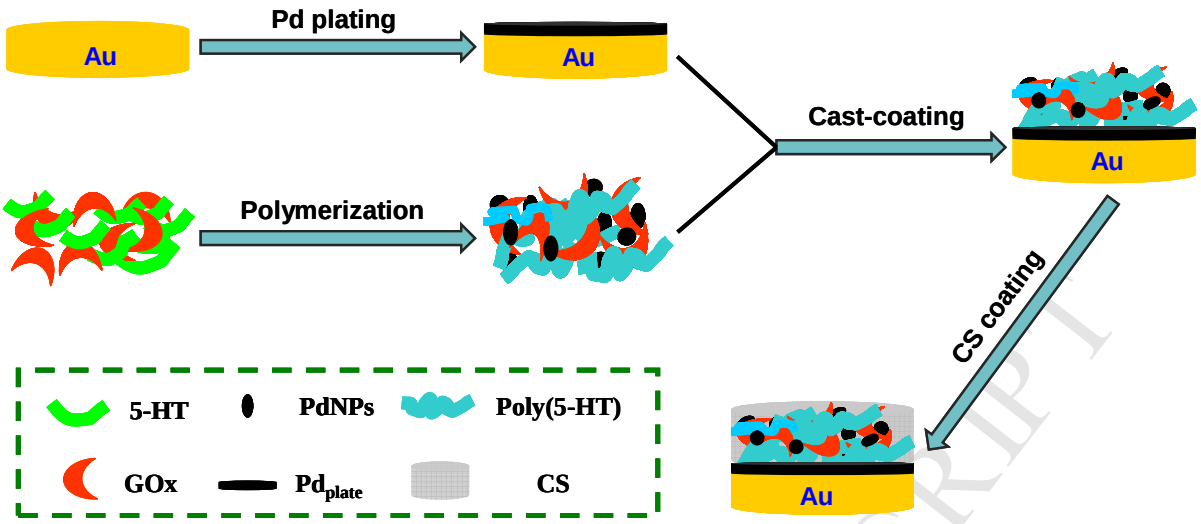

Scheme 1. The construction procedures of the CS/GOx-poly(5-HT)-PdNPs/Pd_{plate}/Au electrode.

Figure captions

Fig. 1. UV-vis spectra and digital pictures (inset) for 40 mM 5-HT (a), 2.5 mg mL^{-1} GOx (b), 2.5 mM Na_2PdCl_4 (c), 40 mM 5-HT + 2.5 mM Na_2PdCl_4 (d), and 40 mM 5-HT + 2.5 mg mL^{-1} GOx + 2.5 mM Na_2PdCl_4 (e, after 30 min reaction and then centrifugation for 8 min at 3500 rpm).

Fig. 2. Cyclic voltammograms (1st (black), 2nd (purple), 10th (red) and 20th (blue) cycles) in phosphate buffer (pH 7.0) containing 5-HT at several concentrations. Scan rate: 500 mV s^{-1}. The 5-HT concentrations are given in the figure.

Fig. 3. SEM pictures of bare Au (a), Pd_{plate}/Au (b), GOx-poly(5-HT)-PdNPs/Pd_{plate}/Au (c), and CS/GOx-poly(5-HT)-PdNPs/Pd_{plate}/Au (d) electrode surfaces, and TEM image of the GOx-poly(5-HT)-PdNPs bionanocomposite (e).

Fig. 4. Chronoamperometric responses to successive additions of glucose (A) and the calibration curves (B) on CS/GOx-poly(5-HT)-PdNPs/Pd_{plate}/Au (a), CS/GOx-PDA-PdNPs/Pd_{plate}/Au (b), GOx-poly(5-HT)-PdNPs/Pd_{plate}/Au (c), CS/GOx/Pd_{plate}/Au (d), CS/GOx-PD-PdNPs/Pd_{plate}/Au (e), Nafion/GOx/Pd_{plate}/Au (f), CS/GOx-PANI-PdNPs/Pd_{plate}/Au (g), and CS/GOx-Na_2PdCl_4/Pd_{plate}/Au (h) electrodes at 0.7 V vs. SCE in pH 7.0 phosphate buffer.

Fig. 5. Cyclic voltammograms and the calibration curves of the anodic peak current (inset) of a CS/GOx-poly(5-HT)-PdNPs/Pd_{plate}/Au electrode in degassed phosphate buffer containing 4 mM BQ and 0, 2, 4, 6, 8, 10, 12, 14, 16, 18, 20, 22, 24, 26, 28, 30, 32, 34, 36, 38 or 40 mM glucose. Scan rate: 50 mV s^{-1}.

Fig. 6. U_{cell} and i_{cell} as functions of R_e (A) as well as j_{cell} and P as functions of U_{cell} (B) for the monopolar

BFC, and time-dependent current responses to successive additions of glucose (C) and the calibration curve (D) for the monopolar BFC.

Fig. 7. Chronoamperometric responses and the calibration curves (inset) on GOx_{chem}/poly(5-HT)-GOx-PdNPs/Pd_{plate}/Au (black) and poly(5-HT)-GOx-PdNPs/Pd_{plate}/Au (red) electrode (A) (electrodeposition protocol), and on CS/GOx_{chem}/poly(5-HT)-GOx-PdNPs/Pd_{plate}/Au (black) and CS/poly(5-HT)-GOx-PdNPs/Pd_{plate}/Au (red) electrodes (B) (chemical protocol) at 0.7 V vs. SCE to successive additions of glucose into pH 7.0 phosphate buffer.

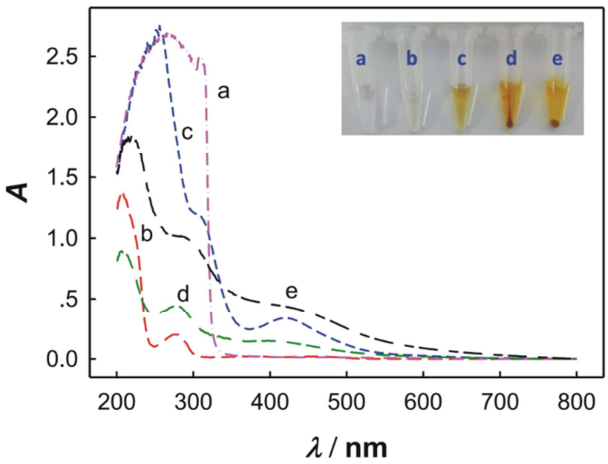

Fig. 1. UV-vis spectra and digital pictures (inset) for 40 mM 5-HT (a), 2.5 mg mL^{-1} GOx (b), 2.5 mM Na_2PdCl_4 (c), 40 mM 5-HT + 2.5 mM Na_2PdCl_4 (d), and 40 mM 5-HT + 2.5 mg mL^{-1} GOx + 2.5 mM Na_2PdCl_4 (e, after 30 min reaction and then centrifugation for 8 min at 3500 rpm).

1

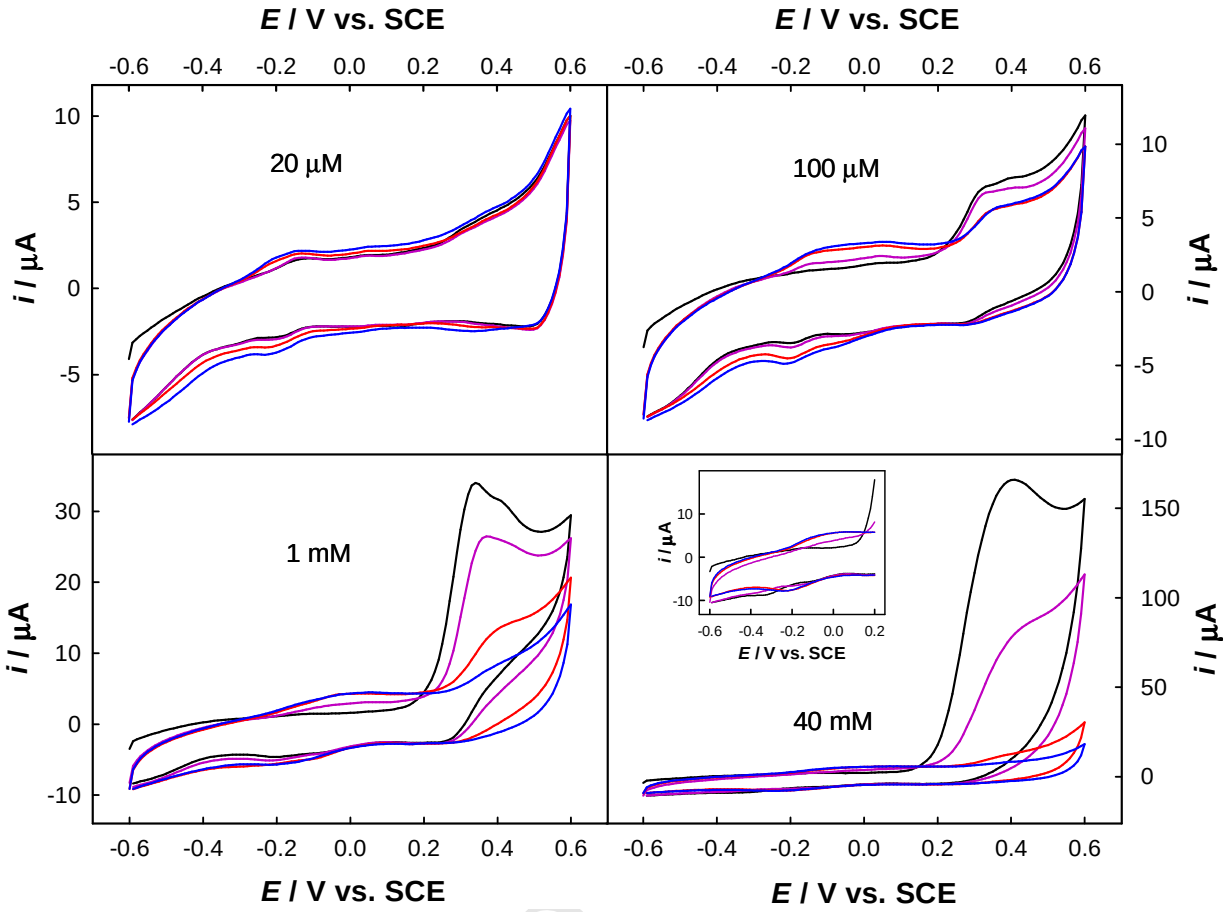

2

3

4 **Fig. 2.** Cyclic voltammograms (1st (black), 2nd (purple), 10th (red) and 20th (blue) cycles) in
5 phosphate buffer (pH 7.0) containing 5-HT at several concentrations. Scan rate: 500 mV s^{-1}. The 5-HT
6 concentrations are given in the figure.

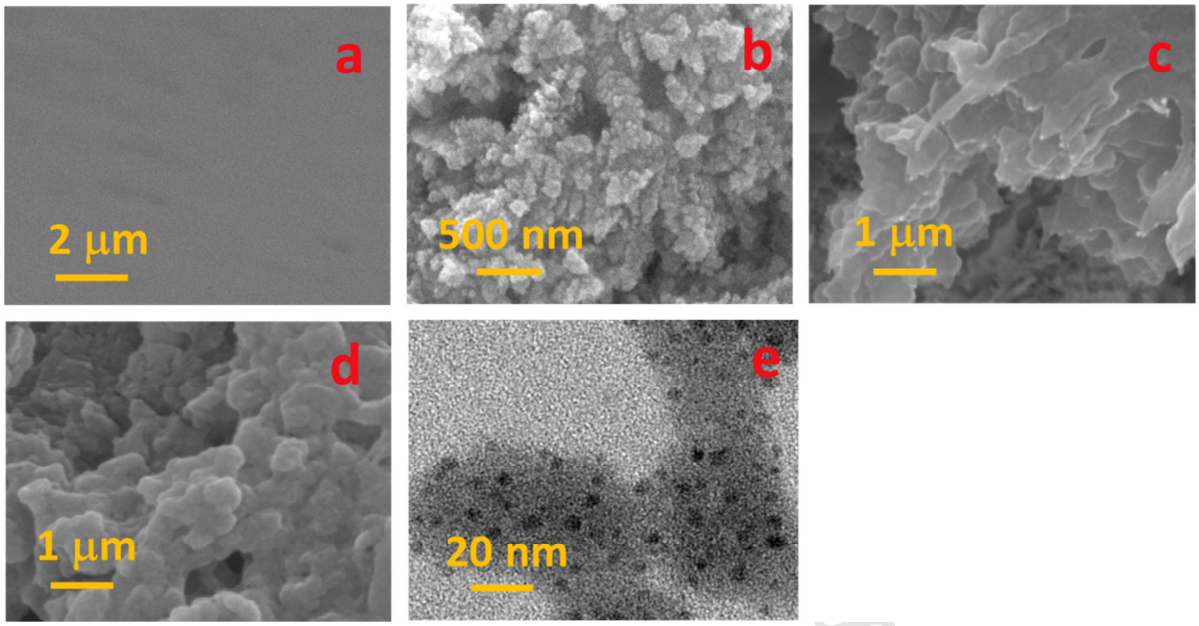

Fig. 3. SEM pictures of bare Au (a), Pd_{plate}/Au (b), GOx-poly(5-HT)-PdNPs/Pd_{plate}/Au (c), and CS/GOx-poly(5-HT)-PdNPs/Pd_{plate}/Au (d) electrode surfaces, and TEM image of the GOx-poly(5-HT)-PdNPs bionanocomposite (e).

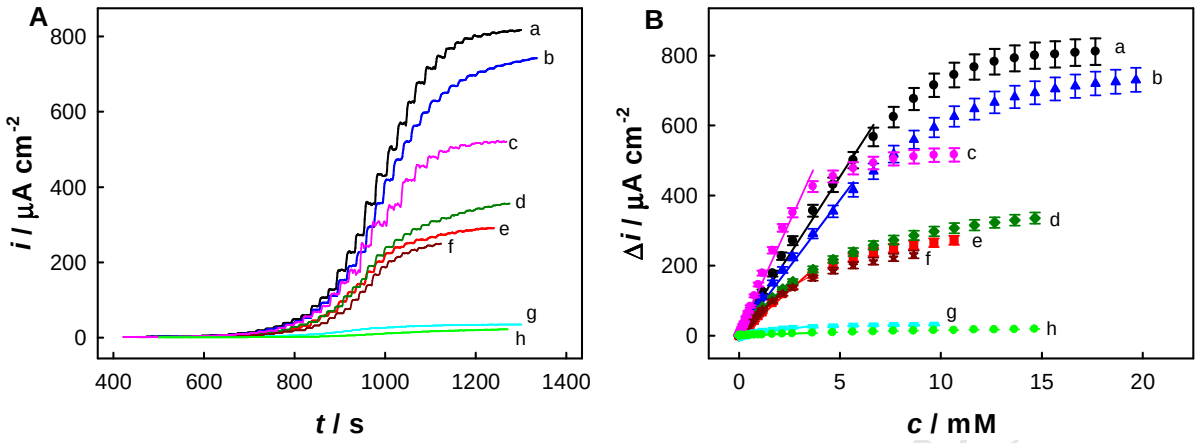

Fig. 4. Chronoamperometric responses to successive additions of glucose (A) and the calibration curves (B) on CS/GOx-poly(5-HT)-PdNPs/Pd_{plate}/Au (a), CS/GOx-PDA-PdNPs/Pd_{plate}/Au (b), GOx-poly(5-HT)-PdNPs/Pd_{plate}/Au (c), CS/GOx/Pd_{plate}/Au (d), CS/GOx-PD-PdNPs/Pd_{plate}/Au (e), Nafion/GOx/Pd_{plate}/Au (f), CS/GOx-PANI-PdNPs/Pd_{plate}/Au (g), and CS/GOx-Na_2PdCl_4/Pd_{plate}/Au (h) electrodes at 0.7 V vs. SCE in pH 7.0 phosphate buffer.

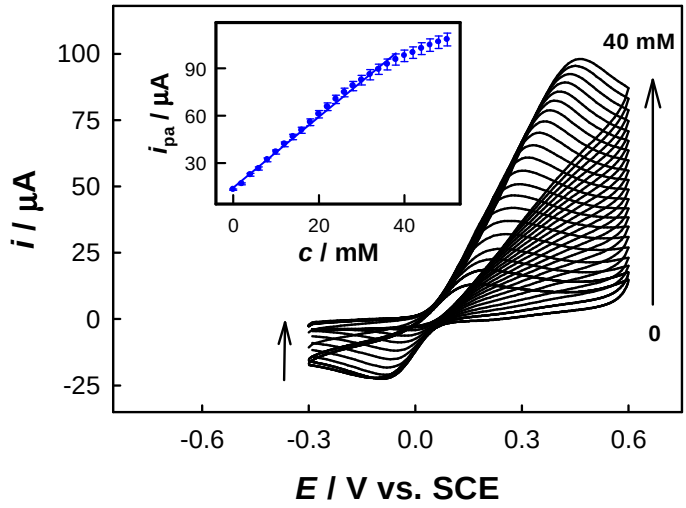

Fig. 5. Cyclic voltammograms and the calibration curves of the anodic peak current (inset) of a CS/GOx-poly(5-HT)-PdNPs/Pd_{plate}/Au electrode in degassed phosphate buffer containing 4 mM BQ and 0, 2, 4, 6, 8, 10, 12, 14, 16, 18, 20, 22, 24, 26, 28, 30, 32, 34, 36, 38 or 40 mM glucose. Scan rate: 50 mV s^{-1}.

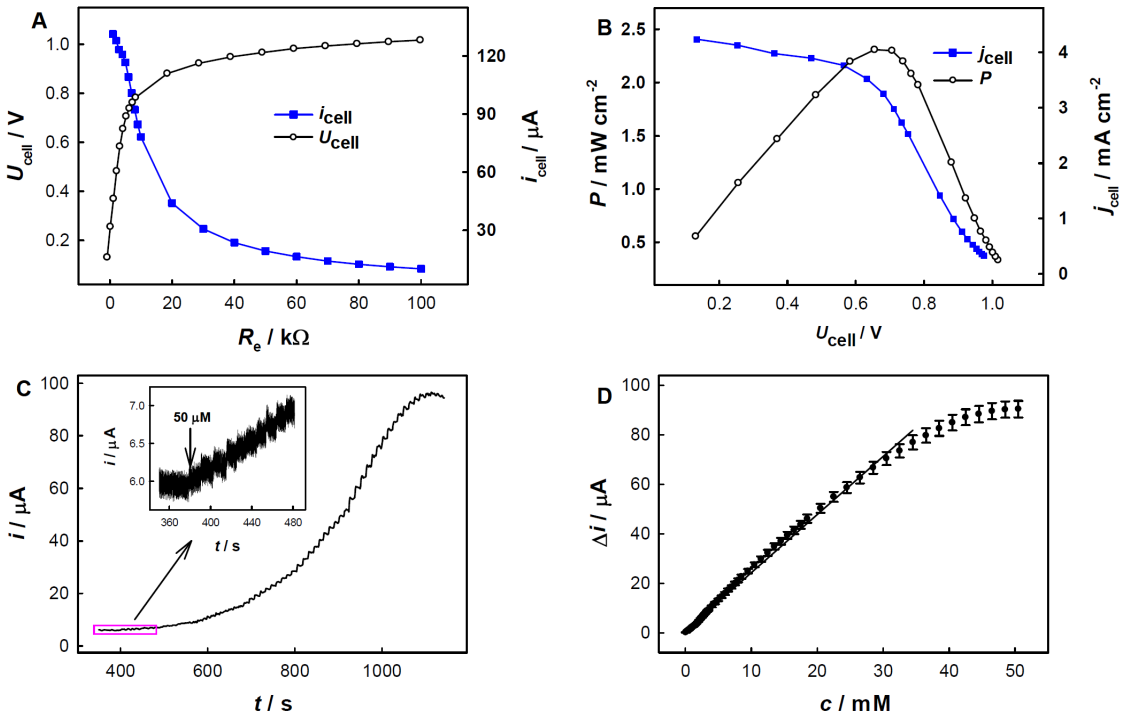

Fig. 6. U_{cell} and i_{cell} as functions of R_e (A) as well as j_{cell} and P as functions of U_{cell} (B) for the monopolar BFC, and time-dependent current responses to successive additions of glucose (C) and the calibration curve (D) for the monopolar BFC.

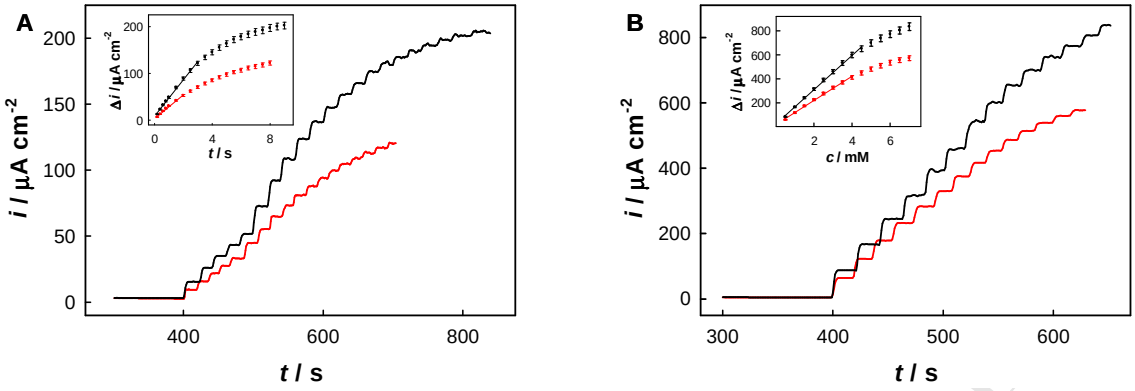

Fig. 7. Chronoamperometric responses and the calibration curves (inset) on GOx_{chem}/poly(5-HT)-GOx-PdNPs/Pd_{plate}/Au (black) and poly(5-HT)-GOx-PdNPs/Pd_{plate}/Au (red) electrode (A) (electrodeposition protocol), and on CS/GOx_{chem}/poly(5-HT)-GOx-PdNPs/Pd_{plate}/Au (black) and CS/poly(5-HT)-GOx-PdNPs/Pd_{plate}/Au (red) electrodes (B) (chemical protocol) at 0.7 V vs. SCE to successive additions of glucose into pH 7.0 phosphate buffer.

Research highlights

► Oxidative polymerization of 5-hydroxytryptamine.

► Immobilization of glucose oxidase.

► Amperometric biosensing of glucose.

► Monopolar glucose biofuel cell as a self-powered biosensing device.

► Physical and chemical dual-immobilization of enzyme.

Electronic Supplementary Material

Oxidative polymerization of 5-hydroxytryptamine to physically and chemically immobilize glucose oxidase for electrochemical biosensing

Ting Huang[a], Zaichun Liu[b], Yunlong Li[a], Yanqiu Li[a], Long Chao[a], Chao Chen[a], Yueming Tan[a], Qingji Xie[a,*], Shouzhuo Yao[a], Yuping Wu[b,*]

[a] Key Laboratory of Chemical Biology & Traditional Chinese Medicine Research (Ministry of Education of China), College of Chemistry and Chemical Engineering, Hunan Normal University, Changsha 410081, China

[b] School of Energy Science and Engineering & Institute of Advanced Materials, Nanjing Tech University, Nanjing 211816, Jiangsu Province (China)

[*]Corresponding authors. Tel: +86-731-88865515.
E-mail address: xieqj@hunnu.edu.cn (Q.J. Xie), wuyp@fudan.edu.cn (Y.P. Wu)

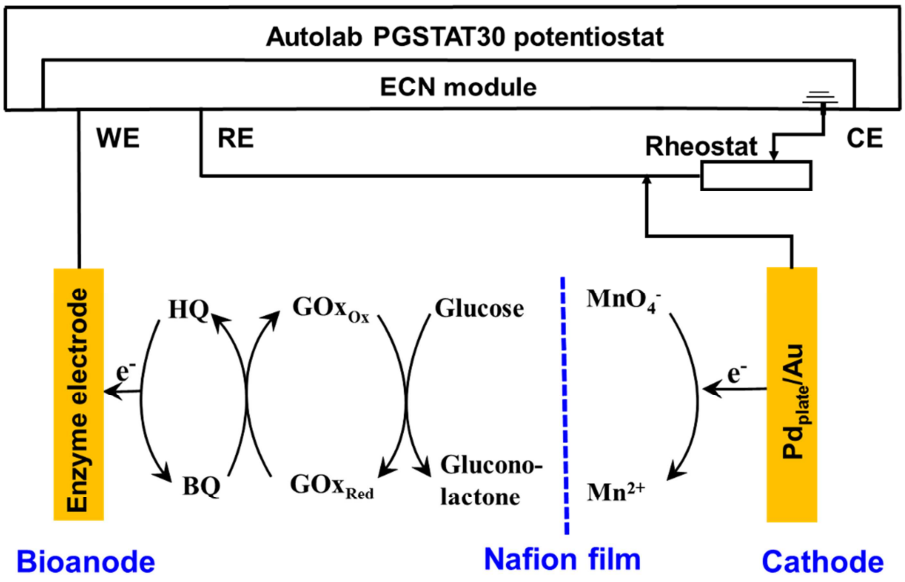

Scheme S1. Schematic diagram of the glucose biofuel cell and electron transfer steps at the cathode and the bioanode.

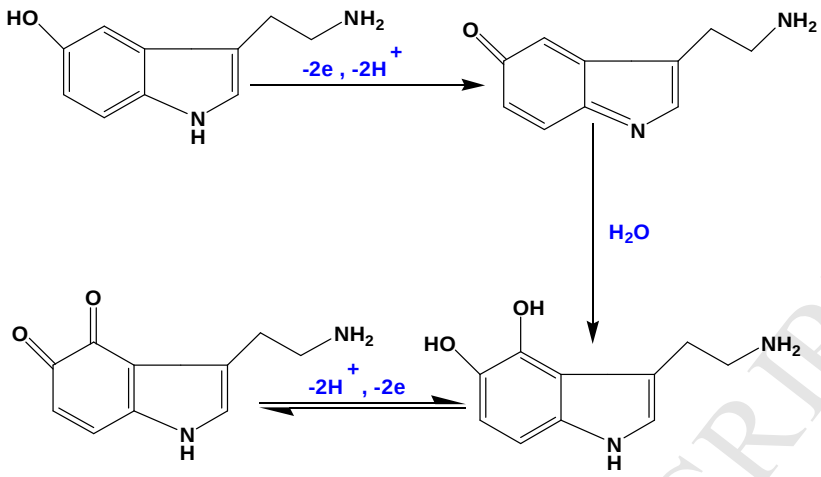

Scheme S2. Possible mechanism for dihydroxyindole formation [1,2].

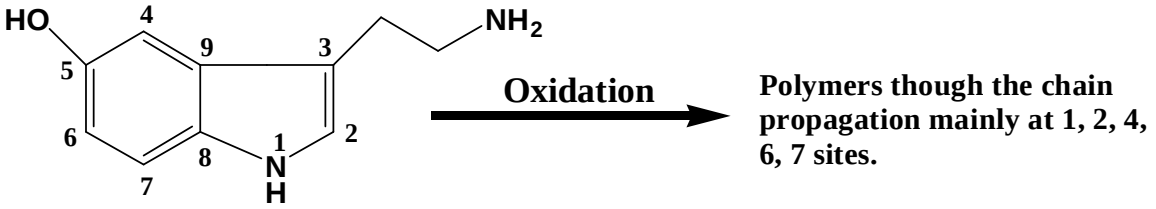

Scheme S3. Possible mechanism for 5-HT polymerization.

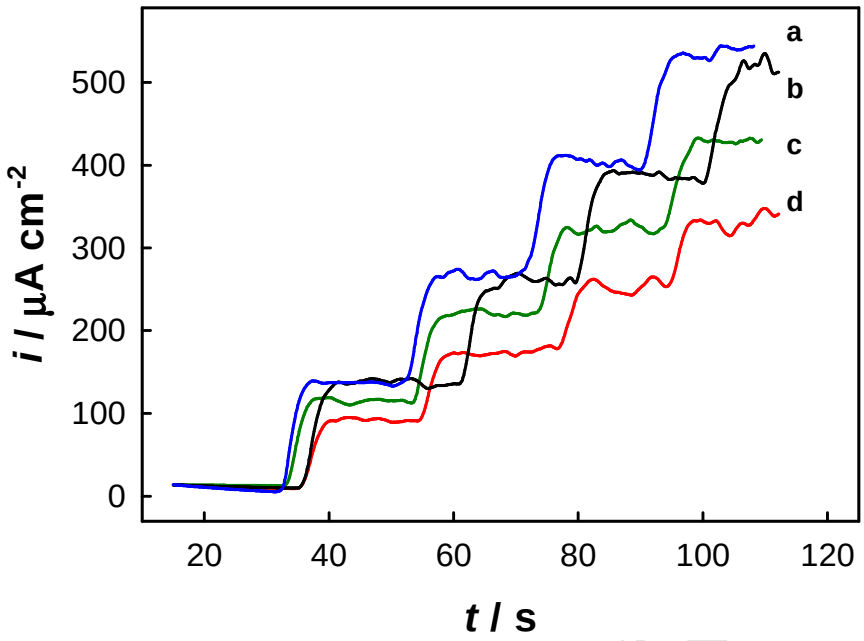

Fig. S1. Chronoamperometric responses on Pt_{plate}/Au (a), Pd_{plate}/Au (b), Au_{plate}/Au (c) and bare Au (d) electrodes at 0.7 V vs. SCE to successive additions of 0.1 mM H_2O_2 into pH 7.0 phosphate buffer. Here, the Pt_{plate}/Au (a) and Pd_{plate}/Au (b) electrodes give the greatest and almost the same anodic current responses, demonstrating the very high electrocatalytic activity of electroplated Pd that is well comparable with that of electroplated Pt.

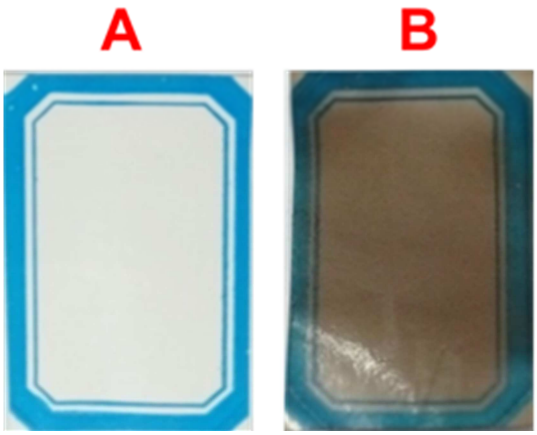

Fig. S2. Photographs of a tagboard before (A) and after (B) casting 100 mM tris-HCl buffer (pH 8.5) containing 40 mM 5-HT for 48 h, drying in air, washing with water, and then drying with a stream of pure nitrogen.

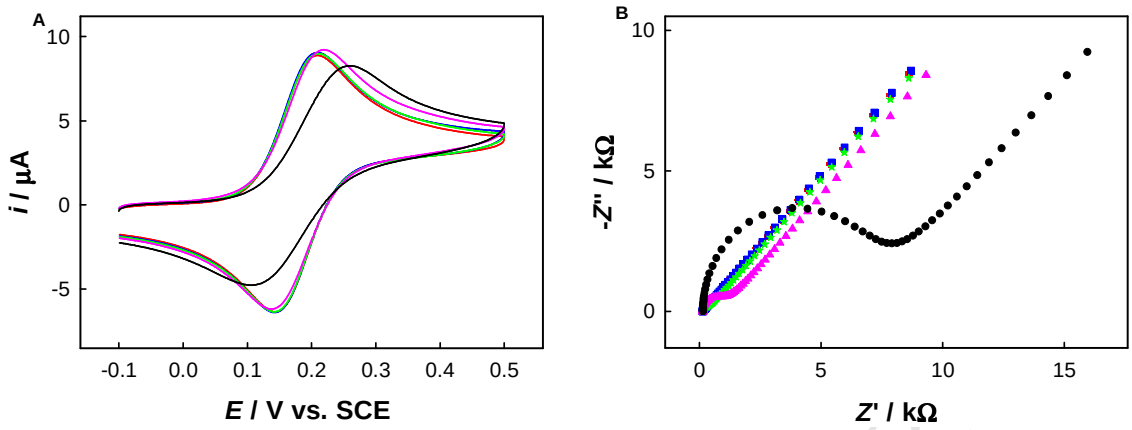

Fig. S3. Cyclic voltammograms (A, scan rate: 50 mV s^{-1}) and Nyquist curves (B, potential applied: 0.176 V; frequency range: 100 kHz-0.01 Hz; amplitude: 5 mV; quite time: 200 s) in 0.1 M K_2SO_4 containing 2 mM $K_4Fe(CN)_6$ at the Au electrodes after experiencing CV treatments in 5-HT-free blank solution (red) or in 5-HT-containing solutions as in Fig. 2 (5-HT concentration: 20 μM (blue), 100 μM (green), 1 mM (pink), and 40 mM (black)). A pair of well-defined redox peaks was observed for electrodes treated at low concentrations of 5-HT (20 μM, 100 μM) and in the absence of 5-HT, indicating the very slightly changed electroactivity of Au electrode here. However, at a medium concentration (1 mM) and especially a high concentration (40 mM) of 5-HT, the peak-to-peak separation became wider, indicating the decreased electroactivity due to electrodeposition of electron-insulating poly(5-HT) on the electrode. The EIS tests have confirmed the conclusions drawn from the above CV experiments. As is well known, the charge transfer resistance (R_{ct}) is a useful parameter reflecting the facility of electrode reaction, which can be measured by EIS from the semicircle diameter in the Nyquist plot. At 20 and 100 μM, we observed small R_{ct} values (below 200 Ω). However, at 1 mM, the R_{ct} of the modified electrode increased to 819 Ω (pink), and at 40 mM, the R_{ct} of the modified electrode increased significantly (black, R_{ct} = 6758 Ω). The above EIS data validate the CV results, both indicating that poly(5-HT) film obtained at high 5-HT concentration has been successfully electrodeposited on the Au electrode surface.

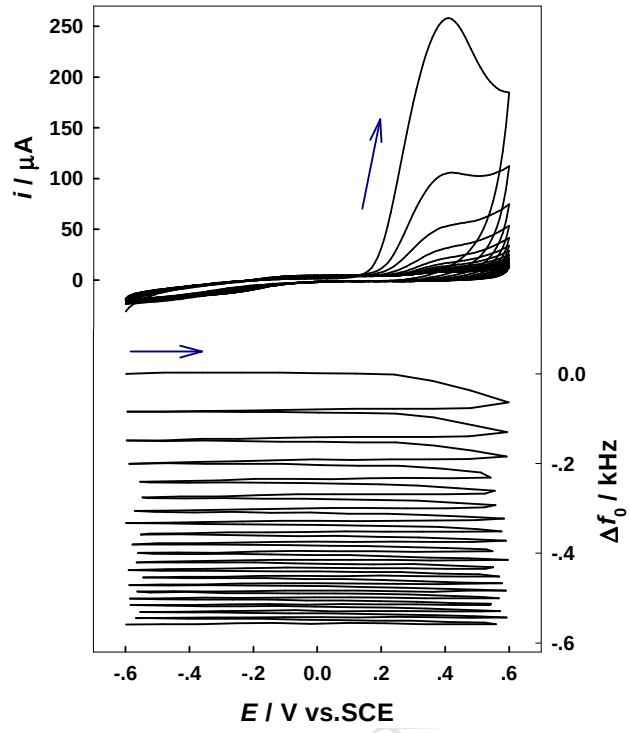

Fig. S4. Simultaneous records of current (i) and Δf_0 during CV treatment of EQCM Au electrode in 0.1 M phosphate buffer (pH 7.0) containing 40 mM 5-HT. Scan rate: 20 mV s^{-1}.

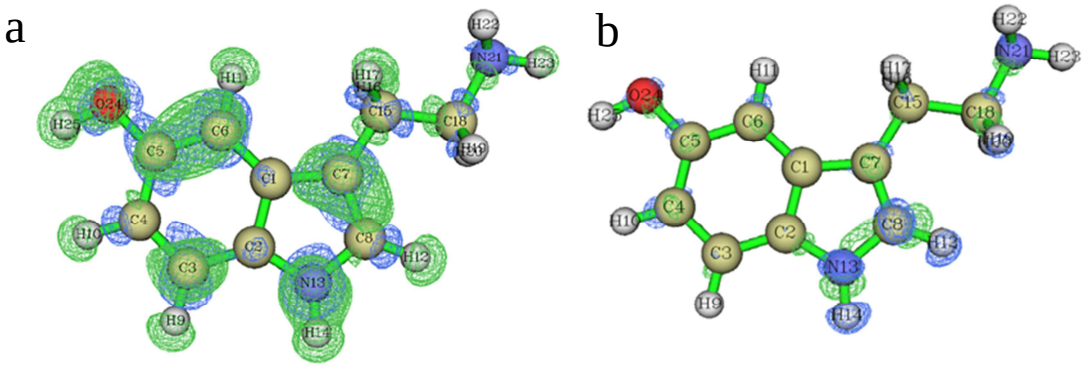

Fig. S5. Fukui function for electrophilic attack (a) and nucleophilic attack (b). The isosurfaces were visualized by Multiwfn software (isovalue = 0.001 a.u.). Gray, white, red, blue represent C, H, O, and N atoms, respectively.

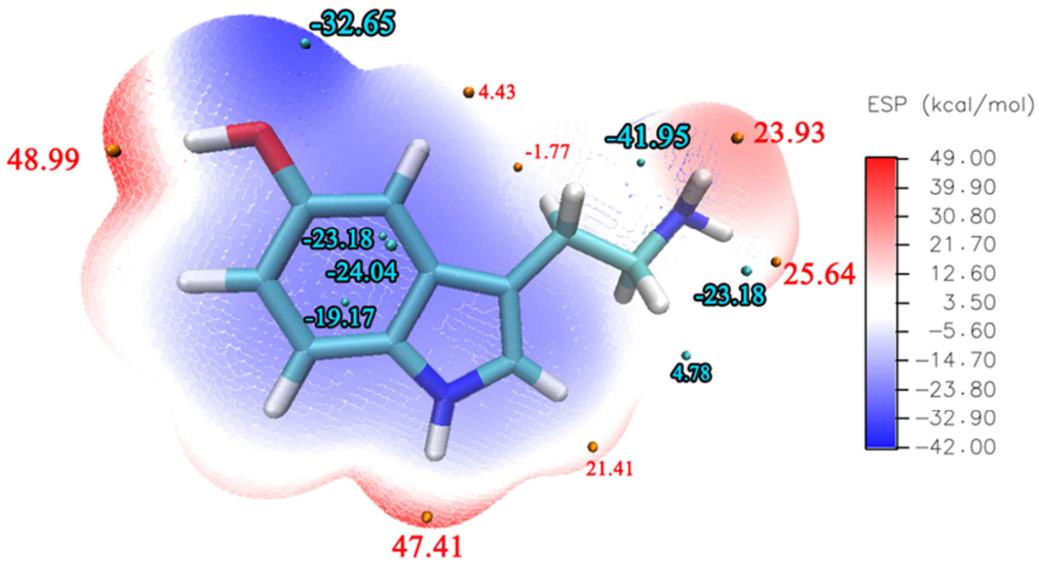

Fig. S6. Optimized structures with color-mapped ESP on vdW surface to 5-HT. In which ESP varying from global minimum and maximum is shown in blue, white and red respectively. Cyan and orange spheres correspond to surface local minima and maxima of ESP, respectively. Cyan, white, red, and blue represent C, H, O, and N atoms, respectively.

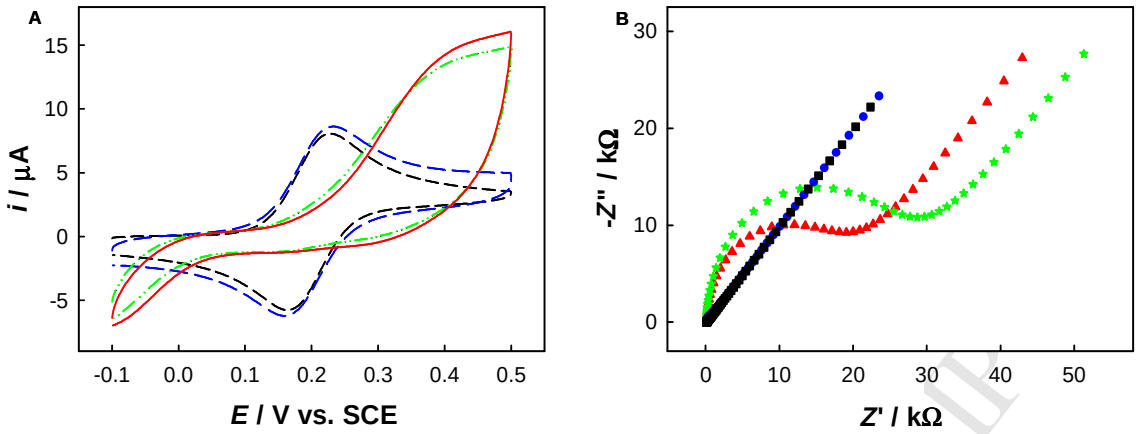

Fig. S7. Cyclic voltammograms (A, scan rate: 50 mV s^{-1}) and Nyquist curves (B, potential applied: 0.192 V; frequency range: 100 kHz-0.01 Hz; amplitude: 5 mV; quite time: 200 s) of bare Au (black), Pd_{plate}/Au (blue), GOx-poly(5-HT)-PdNPs/Pd_{plate}/Au (green), and CS/GOx-poly(5-HT)-PdNPs/Pd_{plate}/Au (red) in 0.1 M K_2SO_4 containing 2 mM $K_4Fe(CN)_6$. A pair of well-defined redox peaks with peak-to-peak separation (ΔE_p) of 65 mV was observed at the bare Au electrode (black), indicating the very high electroactivity of the pretreated bare Au disk electrode. At the Pd_{plate}/Au electrode (blue), the peak current slightly increased and the ΔE_p was 78 mV, demonstrating the high electroactivity and electron-conductivity of Pd_{plate} as well. At the GOx-poly(5-HT)-PdNPs/Pd_{plate}/Au electrode, the redox peaks became almost sightless, indicating the low electroactivity and electron-conductivity of the GOx-poly(5-HT)-PdNPs bionanocomposite. At the CS/GOx-poly(5-HT)-PdNPs/Pd_{plate}/Au electrode, the redox peaks was also invisible. The EIS tests have confirmed the conclusions drawn from the above cyclic voltammetry experiments. At the bare Au (black) and Pd_{plate}/Au electrodes, we observed small R_{ct} values (both below 700 Ω). Cast-coating the GOx-poly(5-HT)-PdNPs bionanocomposite increased the R_{ct} to 24.9 kΩ and the successive CS coating decreased the R_{ct} to 17.0 kΩ. The above EIS data validate the CV results, both indicating that the enzyme film has been successfully modified on the Au electrode surface.

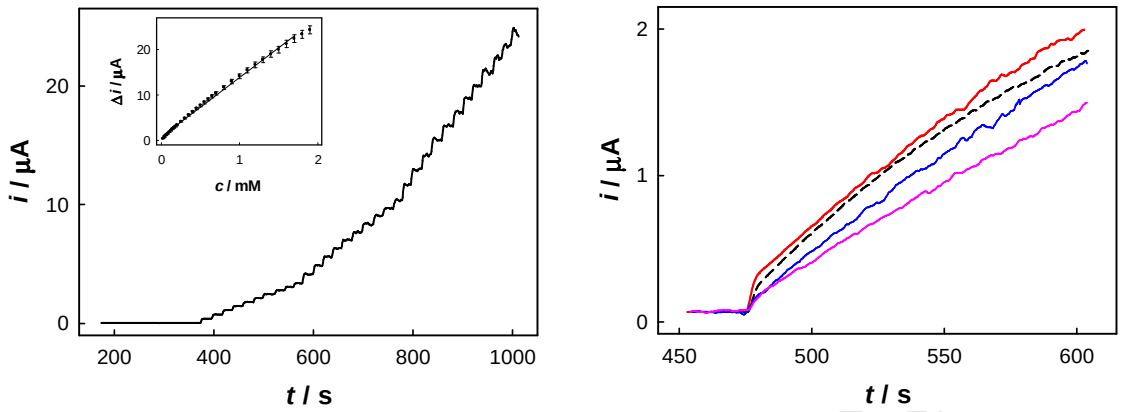

Fig. S8. (A) Chronoamperometric responses and calibration curve (inset, with a linearity regression equation of ΔI (μA) = 13.1c (mM)) of an Au disk electrode potentiostated at 0.7 V vs. SCE to successive additions of H_2O_2 in 10 mL of 0.1 M phosphate buffer (pH 7.0). (B) Chronoamperometric responses of enzymatic kinetics of native (red) and immobilized (entrapped in GOx-poly(5-HT)-PdNPs bionanocomposite (black), GOx-PDA-PdNPs bionanocomposite (blue), GOx-PD-PdNPs bionanocomposite (pink)) GOx on Au disk electrodes at 0.7 V vs. SCE to the addition of 60 mM glucose into 10 mL 0.1 M phosphate buffer (pH 7.0). The mass of added Δm_{GOx} for native and immobilized GOx were both 12.5 μg. We obtained the current change value on the Au disk electrode at 0.7 V vs. SCE in the sequent 60 s as 1.12 μA and 1.05 μA for native and immobilized GOx (entrapped in GOx-poly(5-HT)-PdNPs bionanocomposite), respectively. Hence, $n_{H_2O_2}$ is calculated to be 0.85 μmol for native GOx and 0.80 μmol for immobilized GOx (entrapped in GOx-poly(5-HT)-PdNPs bionanocomposite), according to the calibration curve obtained above and the solution volume. So the values of ESA_n and ESA_i under our experimental conditions are $ESA_n = n_{H_2O_2}/\Delta m_{GOx} = 0.85\ \mu mol/1.25 \times 10^{-5}\ g = 68\ kU\ g^{-1}$ and $ESA_i = n_{H_2O_2}/\Delta m_{GOx} = 0.80\ \mu mol/1.25 \times 10^{-5}\ g = 64\ kU\ g^{-1}$, respectively. Thus, the ERA of the immobilized GOx in the poly(5-HT) case is estimated as $ERA = ESA_i/ESA_n = 64\ kU\ g^{-1}/68\ kU\ g^{-1} \times 100\% = 94.1\%$. Similarly, the ERA values of the immobilized GOx in the PDA and PD cases are estimated as 80% and 65%, respectively.

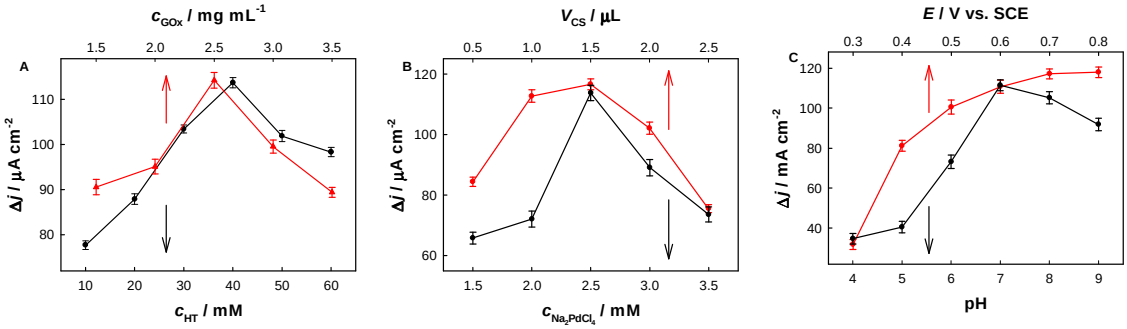

Fig. S9. Optimization of concentrations of 5-HT and GOx (A), concentrations of Na_2PdCl_4 and volume of CS (B) for fabricating the CS/GOx-poly(5-HT)-PdNPs/Pd_{plate}/Au electrode, as well as applied potential and pH (C) for biosensing. The amount of the enzyme cast on electrode is a vital factor affecting the analytical sensitivity of the biosensor. Δi increased and then decreased with the increase of the GOx amount, and the best concentration of GOx was 2.5 mg mL^{-1}, beyond this value, the sensitivity decreased, demonstrating that excessive amounts of enzymes can hinder electron transfer during biosensing. As a reductant, insufficient amount of 5-HT may not produce sufficient Pd nanoparticles to increase the biosensing sensitivity, and the increased amount of insulating poly(5-HT) in bionanocomposite induced by excessive 5-HT can hinder mass/electron transfer during biosensing. So 40 mM 5-HT is selected as the best 5-HT concentration. The optimized concentration of Na_2PdCl_4 is 2.5 mM. The cast volume of 0.30 wt% CS was optimized as 1.5 μL. The effects of pH and applied potential were also examined. The maximum response of the biosensor occurs at pH 7.0 due probably to the highest enzyme activity at this pH. Meanwhile, to minimize interferences and current noise, 0.7 V vs. SCE is selected as the applied potential for amperometric measurement.

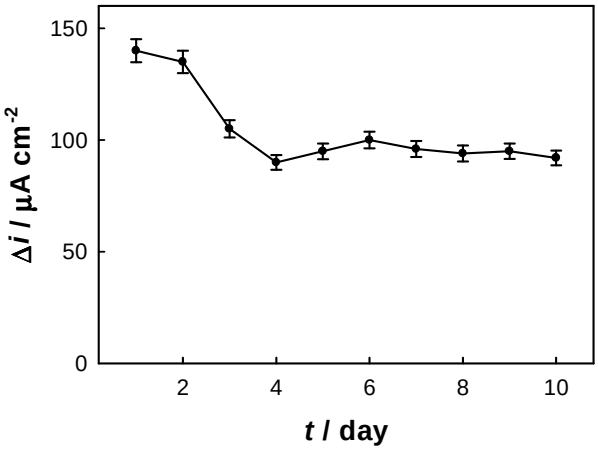

Fig. S10. Storage stability of the GOx-poly(5-HT)-PdNPs/Pd_{plate}/Au electrode under storage conditions. Background solution: 0.1 M phosphate buffer (pH 7.0).

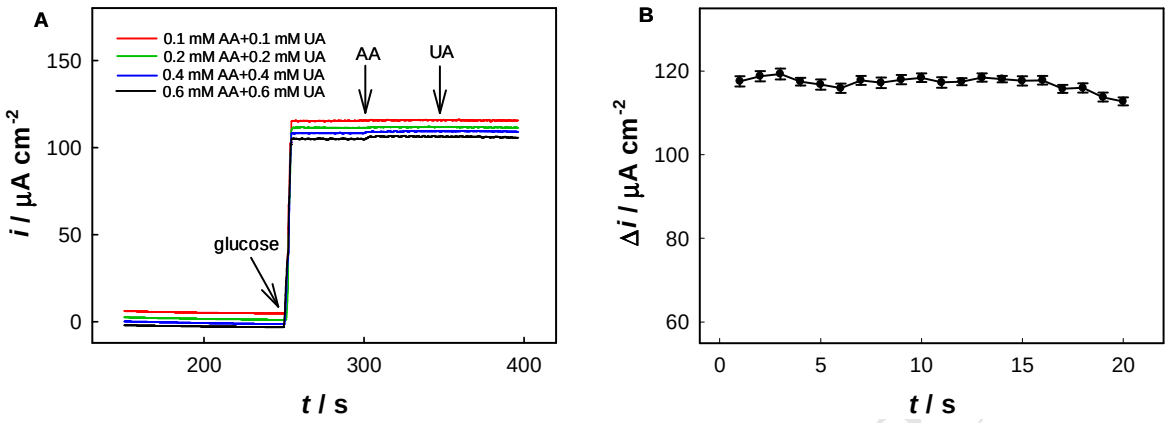

Fig. S11. (A) Effect of additions of 1.0 mM glucose, different concentrations of ascorbic acid (AA) and uric acid (UA) on the response of the CS/GOx-poly(5-HT)-PdNPs/Pd_{plate}/Au electrode. (B) Storage stability of the CS/GOx-poly(5-HT)-PdNPs/Pd_{plate}/Au electrode under storage conditions. Background solution: 0.1 M phosphate buffer (pH 7.0).

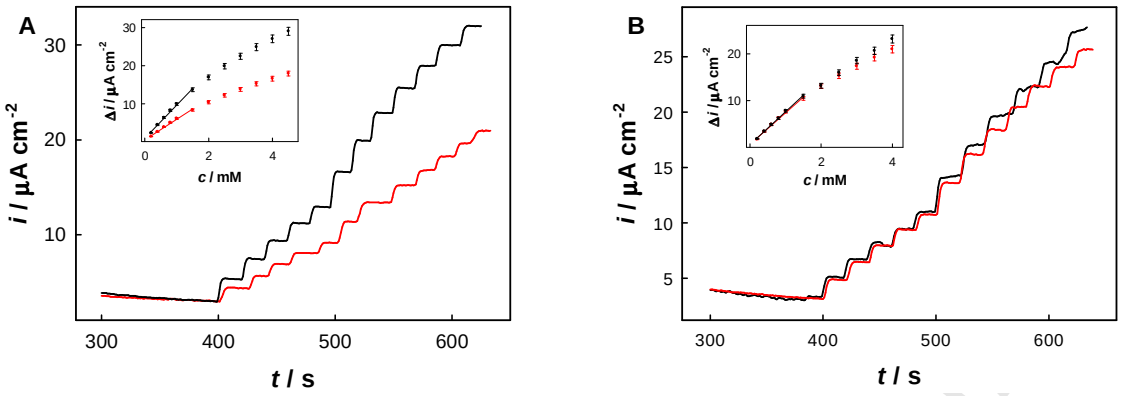

Fig. S12. Chronoamperometric responses and the calibration curves (inset) on GOx_{chem}/poly(5-HT)-GOx/Pd_{plate}/Au (black) and poly(5-HT)-GOx/Pd_{plate}/Au (red) electrode (A), and on GOx_{chem}/PDA-GOx/Pd_{plate}/Au (black) and PDA-GOx/Pd_{plate}/Au (red) electrode (B) at 0.7 V vs. SCE to successive additions of glucose into pH 7.0 phosphate buffer.

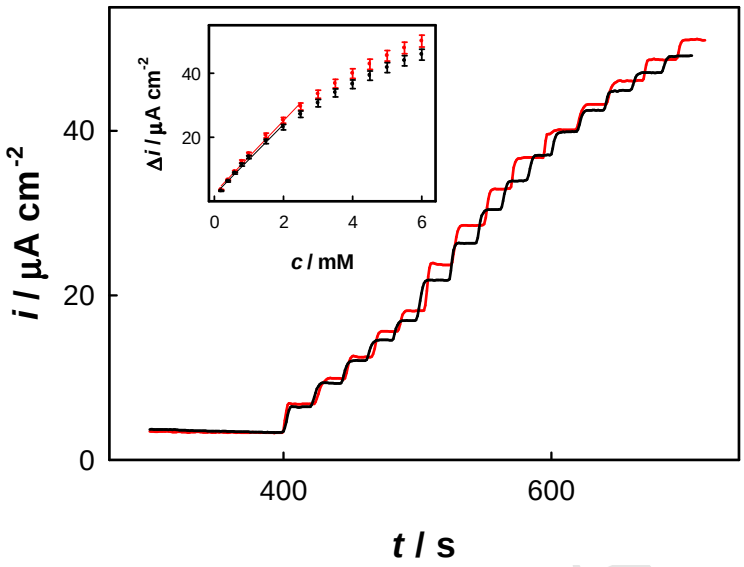

Fig. S13. Chronoamperometric responses and the calibration curves (inset) on GOx/poly(5-HT)-GOx/Pd_{plate}/Au (black) and poly(5-HT)-GOx/Pd_{plate}/Au (red) electrode (A) at 0.7 V vs. SCE to successive additions of glucose into pH 7.0 phosphate buffer.

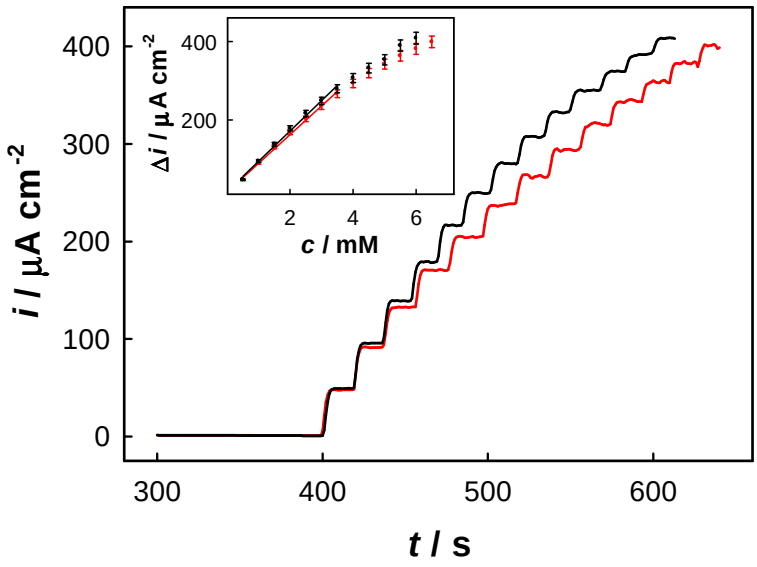

Fig. S14. Chronoamperometric responses to successive additions of glucose and the calibration curves (inset) on CS/GOx$_{chem}$/PDA-GOx-PdNPs/Pd$_{plate}$/Au (black) and CS/PDA-GOx-PdNPs/Pd$_{plate}$/Au (red) electrodes at 0.7 V vs. SCE in pH 7.0 phosphate buffer.

Table S1. The calculated condensed Fukui indices of 5-HT

Atom	N	N-1	*f*-	Atom	N	N+1	*f*+
N13	-0.07182	0.025588	0.097408	H25	0.167648	0.155212	0.012436
C6	-0.065424	0.031972	0.097396	H17	0.030245	0.017364	0.012881
C7	-0.043229	0.04577	0.088999	H16	0.033561	0.019703	0.013858
C3	-0.058459	0.018566	0.077025	H11	0.046174	0.032211	0.013963
O24	-0.209361	-0.132823	0.076538	H10	0.036504	0.018912	0.017592
C5	0.057848	0.134088	0.07624	H22	0.094082	0.07392	0.020162
C8	-0.019273	0.032504	0.051777	H20	0.028853	-0.013266	0.042119
C4	-0.076063	-0.040945	0.035118	H9	0.04251	-0.018912	0.061422
C1	-0.030536	-0.008945	0.021591	H23	0.095092	0.032783	0.062309
C2	0.015755	0.03717	0.021415	H19	0.011803	-0.052691	0.064494
N21	-0.216314	-0.20293	0.013384	H12	0.048705	-0.111059	0.159764
C15	-0.049767	-0.037296	0.012471	H14	0.140623	-0.109575	0.250198
C18	-0.008543	-0.002864	0.005679				

Nucleophilic attack: $f^{+}(\mathbf{r})=\rho_{N+1}(\boldsymbol{r})-\rho_{N}(\boldsymbol{r})$

Electrophilic attack: $f^{-}(\mathbf{r})=\rho_{N}(\boldsymbol{r})-\rho_{N-1}(\boldsymbol{r})$

where *N* is number of electrons in present system, and the constant term *v* in the partial derivative is external potential.

Table S2. Characteristics of some Pd nanomaterials-based glucose biosensors

Fabrication	Sensitivity ($\mu A\ mM^{-1}\ cm^{-2}$)	LOD (μM)	LDR (mM)	Reference
GOx/PdNPs/CS-GR/GCE	32.1	0.2	0.001-1.0	[3]
Nafion/Pd-HCNF/GOx/GCE	13	30	0.06-6.0	[4]
RGO-Pd-GOx/GCE	40.8		1.0-8.0	[5]
Nafion/GOx/Pd-CNT/GCE	40.8	150	Up to 12.0	[6]
GOD/Pt/MWCNT-PANI/GCE	16.1	1.0	0.003-8.2	[7]
CS/GOx-PABA-PdNPs/ Pd_{plate}/MWCNTs/Au	160	0.1	0.002-4.5	[8]
Nafion/PEDOT-Pd/GOx/GCE	1.6		0.5-30.0	[9]
CS/GOx-poly(5-HT)-PdNPs/Pd_{plate}/Au	110	0.2	0.002-6.66	This work
GOx-poly(5-HT)-PdNPs/Pd_{plate}/Au	126	0.2	0.002-3.66	This work
CS/GOx-PDA-PdNPs/Pd_{plate}/Au	87.2	0.6	0.002-5.66	This work
CS/GOx-PANI-PdNPs/Pd_{plate}/Au	10.7	1.8	0.002-1.66	This work
CS/GOx-PD-PdNPs/Pd_{plate}/Au	55.3	3.6	0.005-3.65	This work
CS/GOx/Pd_{plate}/Au	61.0	1.6	0.002-2.66	This work
Nafion/GOx/Pd_{plate}/Au	58.4	2.1	0.005-2.16	This work
CS/GOx-Na_2PdCl_4/Pd_{plate}/Au	2.35	5	0.01-2.64	This work

[a] HCNF: helical carbon nanofiber; PEDOT: poly(3,4-ethylenedioxythiophene); CNT: carbon nanotube; PDA: polydopamine; PANI: polyaniline; PD: poly(L-DOPA).

Table S3. Results obtained in analysis of several human serum samples with CS/GOx-poly(5-HT)-PdNPs/Pd_{plate}/Au*

	Determined by biosensor (mM)	Determined in hospital (mM)	Bias (mM)	Standard added (mM)	Found (mM)	recovery
1	4.52	4.90	-0.38	5.00	5.27	105
2	4.05	4.38	-0.33	5.00	5.15	103
3	4.19	4.38	-0.19	5.00	5.52	110

* Fresh serum samples were first analyzed at Hunan Normal University Hospital with a Biochemical Analyzer (Mindray BS-300, Shenzhen Mindray Biomedical Electronics Co., Ltd.) based on the well-known GOx-peroxidase spectrophotometric method. The samples were then analyzed with the CS/GOx-poly(5-HT)-PdNPs/Pd_{plate}/Au electrode. Serum sample (0.100 mL) was added into 10.0 mL 0.1 M phosphate buffer at pH 7.0, and the current response was recorded at 0.7 V vs. SCE. The concentrations of glucose in serum are calculated from the calibration curve.

References (The numbering here is only for the Electronic Supplementary Material)

[1] G. Dryhurst, Applications of electrochemistry in studies of the oxidation chemistry of central nervous system indoles, Chem. Rev. 90 (1990) 795-811.

[2] B. V. Sarada, T. N. Rao, D. A. T. And, A. Fujishima, Electrochemical oxidation of histamine and serotonin at highly boron-doped diamond electrodes, Anal. Chem. 72 (2000) 1632-1638.

[3] Q. Zeng, J. S. Cheng, X. F. Liu, H. T. Bai, J. H. Jiang, Palladium nanoparticle/chitosan-grafted graphene nanocomposites for construction of a glucose biosensor, Biosens. Bioelectron. 26 (2011) 3456-3463.

[4] X. Jia, G. Hu, F. Nitze, H. R. Barzegar, T. Sharifi, C. W. Tai, Synthesis of palladium/helical carbon nanofiber hybrid nanostructures and their application for hydrogen peroxide and glucose detection, ACS Appl. Mater. Interfaces 5 (2013) 12002-12017.

[5] E. Mijowska, M. Onyszko, K. Urbas, M. Aleksandrzak, X. Shi, D. Moszyński, K. Penkala, J. Podolski, M. E. Fray, Palladium nanoparticles deposited on graphene and its electrochemical performance for glucose sensing, Appl. Surf. Sci. 355 (2015) 587-592.

[6] S. H. Lim, W. Ji, J. Lin, Q. Li, K. Y. Jin, A glucose biosensor based on electrodeposition of palladium nanoparticles and glucose oxidase onto nafion-solubilized carbon nanotube electrode, Biosens. Bioelectron. 20 (2005) 2341-2346.

[7] H. Zhong, R. Yuan, Y. Chai, W. Li, X. Zhong, Y. Zhang, In situ chemo-synthesized multi-wall carbon nanotube-conductive polyaniline nanocomposites: characterization and application for a glucose amperometric biosensor, Talanta 85 (2011) 104-111.

[8] L. Sun, Y. Ma, Z. Pei, C. Long, T. Huang, Q. Xie, C. Chao, S. Yao, An amperometric enzyme electrode and its biofuel cell based on a glucose oxidase-poly(3-anilineboronic acid)-pd nanoparticles bionanocomposite for glucose biosensing, Talanta 138 (2015) 100-107.

[9] P. Santhosh, K. M. Manesh, S. Uthayakumar, S. Komathi, A. I. Gopalan, K. P. Lee, Fabrication of enzymatic glucose biosensor based on palladium nanoparticles dispersed onto poly(3,4-ethylenedioxythiophene) nanofibers, Bioelectrochemistry 75 (2009) 61-66.